TRANSIENT THERMO-MECHANICAL INVESTIGATION OF A SIC-BASED SOLID-STATE POWER CONTROLLER

BY

THEODORE BASIL BALTIS

BS, State University of New York at Binghamton, 2006

THESIS

Submitted in partial fulfillment of the requirements for
the degree of Master of Science in Mechanical Engineering
in the Graduate School of
Binghamton University
State University of New York
2011

Accepted in partial fulfillment of the requirements for
the degree of Master of Science in Mechanical Engineering
in the Graduate School of
Binghamton University
State University of New York
2011

November 29, 2011

James Pitarresi, Chair and Advisor
Department of Mechanical Engineering, Binghamton University

Roy McGrann, Member
Department of Mechanical Engineering, Binghamton University

Seungbae Park, Member
Department of Mechanical Engineering, Binghamton University

ABSTRACT

The Solid-State Power Controller has proven to be the best option for overload current protection in power distribution systems, but this technology is still fairly new and its capabilities have yet to be fully demonstrated. Previous work in the development of these components has been applied piecemeal, focusing on only the capabilities of the devices themselves or on determining the best choice of materials for the power packaging of these components. This research provides first documentation on the behavior of a complete module in response to operating conditions.

A module is presented that is designed to operate at a current rating of $96A_{DC}$ nominal and $960A_{DC}$ maximum fault, and is intended to operate to a junction temperature of 350°C from a 105°C ambient. The module is also designed to sustain operation at the maximum fault current for as long as possible before tripping at the junction temperature. These capabilities are achieved through the use of silicon carbide-based semiconductors and an aluminum-based packaging that provides efficient thermal management.

The characterization of the module is provided by using finite element analysis software to simulate the behavior of the module in response to the maximum fault current. Through transient thermal simulations it was demonstrated that the semiconductors have a sustaining time of 3 milliseconds and that the module is able to dissipate about 80% of the heat that is generated within the active area of the devices.

Thermo-mechanical simulations were also performed to characterize the stress state of the module under these conditions and it was found that all stresses were under their respective material limits. Pre-stress simulations demonstrated the stress state of the module due to the manufacturing process, and harsh environment simulations were also performed to demonstrate that the buildup of stresses limit the module to an ambient temperature of about -38°C.

DEDICATION

This thesis is dedicated to my parents, for they have devoted their lives to helping me get to where I am today. I will always be grateful for their love and support.

ACKNOWLEDGEMENT

I wish to thank my advisor Dr. James Pitarresi for his guidance and support. I also thank him for believing in me and introducing me to the project that provided the basis for my research and thesis.

I also wish to thank Dr. Douglas Hopkins of DensePower, LLC for not only providing the material and partial funding for my research, but also for his insight and encouragement.

TABLE OF CONTENTS

LIST OF TABLES

LIST OF FIGURES

1. Introduction

1.1 Background

Technological advancements in the field of power electronics along with the increased amount of electrical equipment demanded by current aircraft have renewed interest in the development of the More Electric Aircraft (MEA). Although the idea of a more electric aircraft has been studied by military aircraft designers since World War II, this concept has garnered further support in the last two decades and has now become the premier focus for the future of the aerospace and aviation industry [1]. The MEA trend calls for the replacement of traditional mechanical, hydraulic, and pneumatic loads with electric loads to increase performance, reliability, and maintainability [1-7]. Although these improvements offer tremendous overall system benefits, these developments come at the cost of placing greater electrical demands on the on-board Power Distribution System (PDS) [6,8]. These MEA aircraft have complex electrical systems that require an Electrical Load Management Center (ELMC) to determine at any time which loads are mission-critical, flight-critical, or non-critical [9,10], and the Solid-State Power Controller (SSPC) is an integral part of this system [11,12].

The main responsibility of a solid-state power controller is to provide protection for the wires and components in the power distribution system from overload currents resulting primarily from short circuits or arc faults [11,13]. During a short circuit the current may pulse to a value upwards of ten times the nominal current rating and can greatly damage the electrical components within the power distribution system. The SSPC protects these components by quickly interrupting the circuit once the fault current has been detected. This is crucial because some fault currents, such as those resulting from arc faults, are very short-lived and traditional circuit breaker devices are unable to detect these transients [14,15]. To be effective, the power controller needs to be reliable with a fast fault current interruption capability that is accomplished through the use of a solid-state device. The use of solid-state power controllers is necessary for these new high-power, high-current systems for they provide several benefits over their conventional electro-mechanical counterparts [3,8,16-18].

1.2. Circuit Breaker Development and Advantages of the SSPC

1.2.1. History of Circuit Breaker Technology

The technology of electrical system protection devices has been improved upon several times over the past few decades. The first improvement over the traditional circuit breaker was the Arc Fault Circuit Breaker (AFCB), which added electrical arc fault protection to the device by improving the time it takes to sense a spike in current levels. These devices sample the current in sub-millisecond intervals and records when one of these spikes occur, and when the number of spikes exceeds a set amount the AFCB

interrupts the current flow [19,20]. Despite these improvements, the AFCB still lacked monitor and control capabilities and was limited to the slower current interruption speeds of conventional circuit breakers [14].

The next protection device commonly used addressed the issues of remote control, and is suitably referred to as the Remote Control Circuit Breaker (RCCB). In addition to adding remote control capability, these devices decreased the amount of resistive losses produced and were cheaper and lighter than any previous design. Unfortunately, the RCCB shared the same mechanical characteristics as the traditional circuit breaker and therefore its performance is still limited by its current interrupting capabilities [14].

These limitations of conventional circuit protection devices were overcome by the introduction of the solid-state power controller, of which the first patents appeared in the mid-to-late 1980s. These devices utilize power semiconductors for superior capabilities and are necessary for the true realization of a MEA. The advantages of the SSPC are discussed as follows.

1.2.2. Advantages of SSPC Technology

Conventional electro-mechanical circuit breakers disrupt a fault current through the use of a bimetallic element that mimics the effects of the wiring and heats up as a result of the resistive losses in the circuit. As this element heats up it bends until it releases a latch that in turn releases a spring operated mechanism. It is this mechanism that is responsible for separating the movable contacts within the device in order to

interrupt the current flow [21-23]. This does not completely cut off the current, however, as an arc is produced across this discontinuity when the contacts are separated due to the high voltages produced [23]. This arc must also be dissipated before the current can be completely interrupted, so the true fault current interruption time (tripping time) is limited to the speed of the mechanical parts in addition to the time required to extinguish this arc [24].

Initially, this arc was dissipated by drawing the contacts apart until it could no longer be maintained. Over the years this method was improved upon by employing various mediums to extinguish this arc; they included air, compressed air, oil, sulfur hexafluoride, and a vacuum environment [25,26]. Although progress was definitely made, none are as effective as using a solid-state power controller which is able to interrupt a fault current in microseconds – sometimes even in nanoseconds – as opposed to the milliseconds required of conventional electro-mechanical circuit breakers [14,18,24,25]. It is also desirable to completely eliminate this arcing because it causes degradation in the contacts that may adversely affect reliability by causing interruption failure [11,23,24].

The main advantage of a solid-state power controller is the ability to interrupt a current almost as soon as it is detected, which provides for protection of components in the PDS that may be damaged by high currents as well as for protection of the wires and cables connecting these components. High current levels – even those lasting only microseconds – in these lines will cause a great deal of heating due to the resistive

losses and this heating will degrade the protective coatings of the wires, possibly leading to arcing that may damage other components. The fast response time of the solid-state circuit breaker also leads to advantages in weight and therefore cost savings on the aircraft. With the ability to interrupt a fault current before it presents a hazard to the on-board PDS or ELMC, aircraft designers can utilize lower gauge wires that result in volume and weight reduction in the overall electrical system [11,14,28]. Solid-state power controllers are also generally smaller and lighter than their electro-mechanical counterparts, again providing weight and cost benefits [29,30]. This is significant from a performance point of view as well, for in aircraft whose agility is of primary concern, weight savings ultimately deliver a tremendous boost to maneuverability [24].

Solid-state power controllers also offer other benefits over traditional devices. Due to their small size and light weight, they can be easily integrated into the system and placed wherever is most convenient, providing for flexibility that conventional circuit breakers lack. Because the SSPC can be placed anywhere in the system, this allows designers to create an optimal wiring layout [11]. SSPCs also possess remote-control capability, which allows them to be remotely reset after tripping and for performance to be monitored and controlled in real-time by means of a man-machine interface [4,11,14,23,31]. Also, because these devices do not utilize any moving parts, solid-state power controllers are less susceptible to vibrations than electro-mechanical circuit breakers, further enhancing reliability [14].

1.3. Literature Review

Through the years, PDS protection devices have improved considerably but none are nearly as effective as the solid-state power controller and none but the SSPC are capable of handling the high current loads called upon in the MEA trend. Although the advancement of these PDS protection devices is so crucial, only the electrical capabilities and behavior of solid-state power controllers have been heavily studied and documented so far, and there has yet to be much done in terms of the thermal or mechanical behavior of these devices during operation. In fact, a great deal of research in this field has focused on determining the role of the SSPC in the overall PDS (where and how it would implemented) [12,32] and how its development is crucial to the fulfillment of the MEA [4,10,33]. Virtual bench tests of a PDS have been conducted to demonstrate the overall system performance benefits and the feasibility of incorporating SSPCs into a more electrical system [2,8,11,17].

For the most part, research on SSPCs has been primarily focused solely on developing and demonstrating the characteristics and capabilities (mostly the fault current interruption ability) of the devices themselves [13,16,18,34-38] with little consideration given to the packaging of these components and how the performance of these components may be affected by this packaging. Most of the work performed on these devices up until now has been limited to determining the minimum trip time possible and the extent of resistive losses (sometimes referred to as “switching losses” in these power switching devices) that occur during this short time, such as in the

research performed by General Electric (GE) and Microsemi on MOSFETs of their own designs [39,40].

Most of the work done in the thermal field has only related to the properties and general behavior of MOSFETs and other power switching devices in response to overall temperature changes. An example is the work done by Data Device Corporation (DDC) where they tested the reliability of their own SSPC through temperature cycling and at different current levels [11]. DDC was able to demonstrate a high reliability in their design, and this is important to verify and document for implementation purposes, but this work does not address the more important issue of the heat produced by the device itself during operation due to resistive losses.

As previously stated, the MEA trend calls for aircraft with more electrically-driven loads, and although this movement has great performance, weight and cost savings benefits, it comes at the expense of a greater electrical load on the PDS and ELMC. Consequently, great emphasis has been placed on the ability of the SSPC to operate at much higher current levels. In the past decade or so, power controller modules have been designed to operate at increasingly higher current levels. As recently as 2005, North Carolina State University demonstrated the capabilities of a module that operated at a nominal rating of $50A_{DC}$ and a maximum fault current rating of $600A_{DC}$ [16]. Even more recently, in 2010, GE demonstrated a module designed to operate at a nominal current of $150A_{DC}$, but this module could only achieve these power

capabilities by utilizing ten MOSFETs in parallel, limiting the power density to a current rating of only 15A per die [39].

Although research focused on packaging concerns is more difficult to come by, initial work has been done to study the thermal effects on power packaging. The University of Arkansas has provided guidelines for power module design based upon the parameters of active device power dissipation, junction temperature, thermal conductivity, and the mismatch of the coefficient of thermal expansion between packaging layers [41]. Although this work identified all of the critical design parameters it did not present any experimental or simulative results, and is intended only for use as an overall design guide.

While much research in the field of high-temperature packaging has focused on testing one material at a time [42-44], there have been some initial packaging studies of the effects of heating on substrates when bonded together [45,46]. The packaging used in the research of [45,46] consisted of Direct Bonded Copper (DBC) substrates on an Aluminum Nitride (AlN) ceramic with an Aluminum Silicon-Carbide (AlSiC) baseplate. The packaging was subjected to thermal cycling between -30°C and 180°C and the main causes of failure were determined to be solder delamination and ceramic fracture. The same experiments were then performed with Direct Bonded Aluminum (DBA) substrates and the results indicated that the aluminum behaved very well under the thermal cycling but concern was expressed over the higher CTE of aluminum as compared to copper. This work is useful in determining which materials may be better-suited for

packaging applications and which modes of failures may be expected, but it – like all other published works – only provided an overall look at the behavior of the packaging layers and does not investigate the performance of the module layers under operating conditions with a power device. In fact, these tests did not include any type of semiconductor as part of the module at all.

Although very necessary, most research on power controller technology has been applied piecemeal, focusing only on certain aspects of the power switching devices or on individual layers of the packaging. The first efforts to pull all of these facets together have been performed by DensePower, LLC, who has taken all of the previous work in different areas and brought it together to focus on the electrical and thermal behavior of a SSPC module in response to the operating conditions, namely the resistive losses. This module has been specifically designed for efficient heat spreading and thermal stress management through the use of aluminum-based packaging and SiC-based MOSFETs, and has been designed to operate up to a junction temperature of 350°C, which is significantly higher than any other module in development [24,47-49]. While most research on SSPCs has been focused on the minimum achievable current interruption time, the work by DensePower has built upon these capabilities and instead focused on the sustaining time of the switching devices at the maximum fault current before reaching the junction temperature. The specific goal of the company is to create a module with the largest sustaining time possible, and this parameter is defined by the ability of the module to draw heat away from the semiconductors during operation, which is directly dependent upon the thermal management capabilities of the module.

DensePower has thoroughly investigated the electrical properties and capabilities of their modules [50,51] and now has recently been delving into documenting the thermal behavior of their power controllers [24,47-49]. Because the research of the company is focused on studying the behavior of their SSPC modules in response to resistive losses, its results are heavily reliant upon the dynamically changing on-state resistance of the semiconductors in the modules (which directly determine the magnitude of these resistive losses). Although this work is innovative, DensePower has been unable to incorporate an efficient model for representing these dynamic resistive losses and therefore its ability to accurately characterize the thermal behavior and to determine the sustaining time of its modules has been limited. The company also has designed the power packaging with thermal stress management as a concern, but has yet to actually investigate the mechanical response of their modules.

1.4. Objective

The work presented in this research was performed in conjunction with DensePower, LLC in an effort to further develop their high-current solid-state power controller. This research is based upon work supported by The United States Naval Air Warfare Center under contract "Intelligent, Fault Tolerant, and Robust Power Management for Aircraft Applications," No. N68335-11-C-0159. The solid-state power controller in development under this contract and through this research is primarily intended for use in the F-35 Lightning II, more commonly known as the Joint Strike Fighter, but also has applications in smart-grid or micro-grid systems [48].

Previous work completed by DensePower, LLC focused on modules utilizing MOSFETs measuring 4.1mm x 4.1mm, and very limited work was performed on modules with a larger set of dies that measure 7mm x 8mm [47]. This research concentrates only on the module consisting of these larger dies which can tolerate much higher current ratings. The goal of this work is to improve and then build upon that initially performed by DensePower, LLC. This was done by reconstructing the models and simulations in order to provide a more accurate account of the transient behavior of the module in response to a fault current.

Because there has been extremely little investigation into the thermal and mechanical behavior of these solid-state devices, this research is presented as more of a first report on the behavior of a specific solid-state power controller with capabilities that exceed those of any other module in currently being developed. The first goal of this work is to accurately determine the maximum sustaining time of the MOSFETs, which is the maximum allowable operating time before reaching the junction temperature. From determining the sustaining time of the module it is possible to calculate how much energy the semiconductors produce during operation, and comparing this value to the amount of energy actually absorbed by the power switches allows for quantification of the thermal management capabilities of the module (i.e. how much heat is being dissipated through the module). An improved thermal characterization of the module will be provided in addition to first documentation on the mechanical behavior (i.e. thermal stresses) of the module. This work also

investigates the pre-stresses in the module as well as the mechanical response of the module when subjected to temperatures as low as -65°C.

1.5. Methodology

With no physical prototypes of the module with larger dies, all studies and characterization of the module were performed through simulation work. Technical specifications were provided by DensePower, LLC so that an accurate model of the solid-state power controller could be built and simulations could be performed using Finite Element Analysis (FEA) software.

In order to attain accurate and credible results from the simulations, it was necessary to faithfully represent the operating conditions of the module. An important aspect of this is the loading conditions, specifically how heat is generated in the MOSFETs. Using the known input current values and the relation to heat generation, an equivalent heat generation rate was determined that is based on the temperature dependence of the semiconductor resistance. This allowed for a true representation of the thermal behavior of the entire module. Transient thermal simulations were performed to determine the maximum sustaining time of the MOSFETs and this result was used to determine the amount of energy that is produced before the switching devices reach the junction temperature. These values were used to quantify the thermal capabilities of the module.

Transient simulations were also utilized to investigate the mechanical behavior of the module in response to a fault current. By including material properties such as

Young's Modulus and the coefficient of thermal expansion, the thermal stresses in the module layers could be examined and compared to the limits of their respective materials. Steady-state simulations were then performed to determine the stresses in the module due to the manufacturing process (pre-stresses) and due to the influence of very low ambient temperatures.

2. Features of the Proposed SSPC Module

The solid-state power controller in development by DensePower, LLC utilizes four silicon-carbide (SiC) based metal-oxide-semiconductor field-effect transistors (MOSFET) running in parallel to operate at a nominal current rating of $96A_{DC}$ and be able to protect against a fault current rated as high as $960A_{DC}$, which is ten times higher than the nominal rating. Operation at these currents makes it the highest-density power module currently in development. As previously mentioned, these high-power capabilities are achieved through the use of two main techniques; each of which are discussed in detail as follows. A rendering of the complete module is provided below in Figure 2.1.

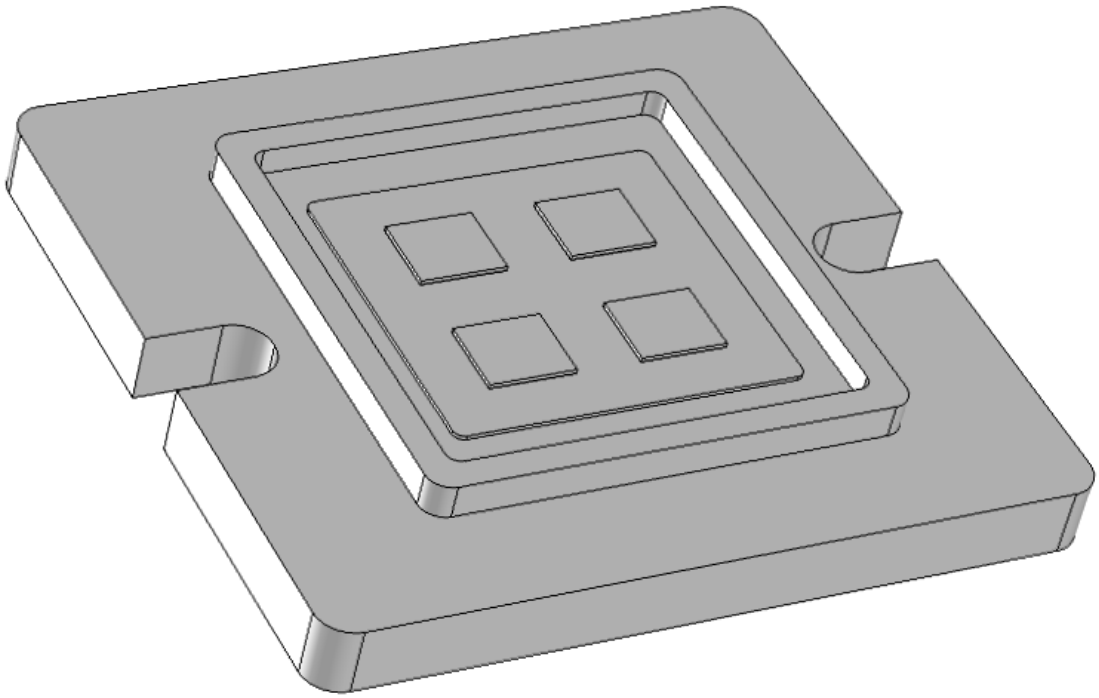

Figure 2.1. Complete Solid-State Power Controller Module

2.1. SiC Over Si

The power switching device of the solid-state power controller presented in this research is a 4H silicon carbide MOSFET manufactured by Cree, Inc. SiC devices, in addition to those based on other wide bandgap materials such as gallium nitride (GaN), have become increasingly utilized in power electronics as applications with higher power requirements have pushed traditional silicon (Si) devices to their limits [52]. A SiC semiconductor was chosen because its capabilities far exceed those of silicon for high temperature applications. There are around 150 polytypes of SiC, but only two of them – 6H and 4H – are commercially available. 4H SiC is the most commonly used polytypebecause of the isotropic nature of its electrical properties [52,53]. The main

advantages of SiC are its wide bandgap energy, high electric breakdown field, and high thermal conductivity [31,34,36,55].

The wide bandgap energy of SiC-based components allows them to operate at higher temperatures without losing their electrical properties. As temperature rises, electrons within the material increase in thermal energy and wish to move between bands that are naturally present within the material. The energy required for jumping between bands is determined by the amount of space between them, so materials that are considered "wide bandgap" (materials with a larger gap between bands) are able to rise to higher temperatures without their electrons moving around [52]. Si-based devices are limited to operation temperatures of about 150°C, while literature has stated that SiC-based devices can operate at temperatures up to 600°C [36,52,55,57]. The wide bandgap energy also results in higher radiation hardness for SiC devices [29,52].

The higher electric breakdown field of SiC devices allows for thinner, higher doped blocking layers which effectively lower the on-state resistance [29,54]. The lower on-state resistance results in less power dissipation in the active device, which ultimately amounts to less heat being generated in the device during operation [11,31]. Because the proposed module is to operate at such high currents and its operation is ultimately limited by a pre-determined junction temperature, it is important to use a material that will produce as little heat as possible.

Although the amount of heat generation is reduced by utilizing a SiC semiconductor, the eventual accumulation of heat and a rise in temperature is unavoidable. Because of this, the higher thermal conductivity of SiC as compared to Si is extremely important. The higher value in the SiC device is directly attributed to the strong silicon to carbon covalent bond that is not possible in a solely Si-based device [29]. A higher thermal conductivity provides for better thermal management in the device, resulting in more heat being conducted away from the active region and therefore a slower heating rate and temperature rise in the device [36]. This slower heating rate allows for operation at higher power densities [7,39].

Often overlooked, another important advantage of SiC is that it has a thermal expansion coefficient (CTE) that better matches that of the substrates now commonly used in packaging [24,57]. A closer matched CTE provides for better stress management in the device as a result of the thermally-induced strains during high temperature operation.

While the use of silicon carbide-based devices is practical for several reasons, there is one disadvantage to using this material. The downside is that SiC-based devices are more costly to manufacture than those that are Si-based [52,53], but this downside is far outweighed by the performance advantages that these devices bring. The combination of these qualities makes silicon carbide an ideal candidate for high temperature applications such as the one this module is developed for.

2.2. Aluminum-Based Packaging

As previously mentioned, the use of a SiC semiconductor reduces the amount of heat generated in the device as a current is passed through it during operation, but the temperature will still rise in the device. In order to slow down this heating rate, the device is attached to a power package specifically designed to draw heat away from the device. Efficient thermal management will allow the power controller to operate for as long as possible under maximum fault current conditions before reaching the junction temperature, therefore ensuring that the device will not prematurely trip. In this module, the management of heat flow is accomplished through the use of a mono-material approach in the packaging. In an effort to achieve a near uniformity of material properties through the entire module, all of the materials used in this power package are aluminum-based. The composition of the module is further discussed as follows.

The complete power package is composed of the silicon carbide devices that are mounted on a continuous aluminum trace pad that is cast onto an aluminum nitride ceramic which is co-captured in an aluminum metal matrix composite (MMC) baseplate. A stack-up diagram of the module layers can be seen below in Figure 2.2. The exact composition of the baseplate is propriety to DensePower and has been requested not to be discussed, but is always described as being similar to the common MMC aluminum silicon carbide (AlSiC). This aluminum-based packaging was specifically designed for better management of the generated heat and the associated mechanical response of the entire package. Because each layer is aluminum-based, there is a near-uniformity of

thermal conductivity through the layers that promotes steady distribution of heat away from the operating device. Being a ceramic, the AlN layer also serves as a good electrical insulator. Also, due to aluminum's relatively low Young's Modulus, this layer provides a substantial stress relief during temperature cycling [47,50].

In power packaging, another important design parameter is the coefficient of thermal expansion (CTE). The CTE is a property that is a measure of how much a material will contract or expand in accordance with heating or cooling, or otherwise thought of as any change in temperature. It is desirable to match the CTEs of each material in the package as closely as possible in order to reduce the stresses that are developed during temperature transients, therefore increasing the overall reliability of the packaging and the module [41]. The use of all Al-based materials also allows for a better match of the coefficient of the CTE between each layer and allows for better management of the stresses produced in each layer as they contract and expand due to temperature changes.

Another concern in the packaging relates to the forces produced at the boundaries between bonded layers as a result of the expansion/contraction of the layers during operation. The closer match of CTEs between the bonded layers helps to alleviate these forces, but the Al-based structure also provides for a common metallurgical bonding medium between the layers that creates a stronger bond [48,50]. Through the use of the all aluminum-based packaging, we are able to better match the

thermal expansion coefficients and develop stronger bonding between the layers which work in tandem to deliver a higher reliability in the packaging.

Although this aluminum-based packaging was found to be superior to other options such as the more conventional use of copper, it is not without its drawbacks. The electrical resistance of Al is 2.5 times greater than copper and has 40% lower thermal conductance. In order to achieve equivalent power dissipation, the aluminum conductor needs to be 2.5 thicker. This is not a large concern, however, as the absolute value of the thermal resistance is not large and the thicker conductor provides for better stress management in the module [50,51].

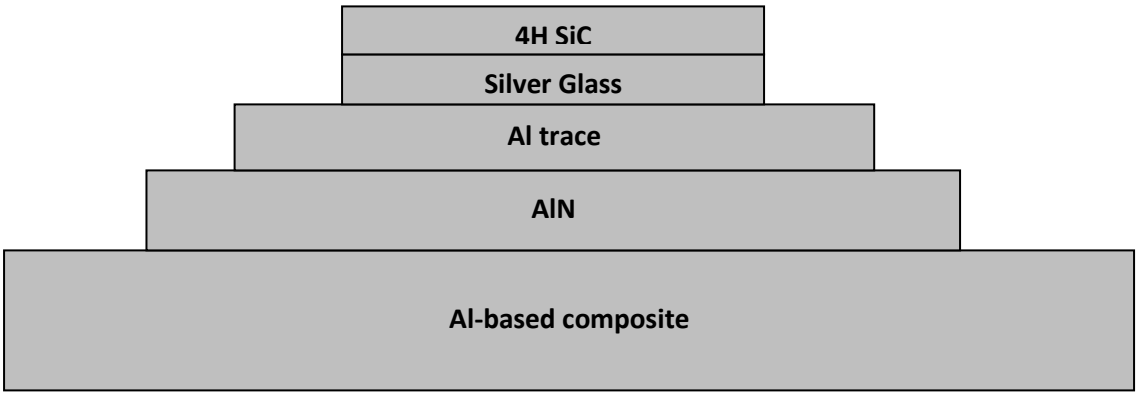

Figure 2.2. Stack Up of SSPC Module Layers

The last component of the module is the die-attach material. The SiC semiconductor switch needs to be bonded to the Al trace layer with a material that is electrically conductive and that is able to withstand the high temperature cycling while also managing the stresses between the die and the aluminum layers. While several materials were considered, the Hysol QMI3555R silver-glass composite was found to be superior to be the superior choice due to its ability to operate at high temperatures, its

relatively higher thermal conductivity and lower coefficient of thermal expansion. Other factors weighing in on this decision were that the material has a low electrical resistivity and proved to be easy to process and void free when applied [50,51].

2.3. Behavior of the SSPC

2.3.1. Electrical Behavior of SSPC (i^2t Trip Protection)

A typical solid-state power controller follows an i^2t (where i is current and t is time) trip-current profile such as the one presented below in Figure 2.3. The curve represents the behavior of the device by demonstrating when protective measures are taken by the power controller according to the current level as a function of time. Based on simulation results and testing, this profile is built and assigned to the SSPC. During operation, the SSPC samples current input in real time and compares it to its own i^2t profile [8,54]. When the sampled data is below the curve the switch in the device keeps the circuit closed and operating, but when this sampled data falls above the curve the switch in the device opens in order to interrupt the current flow. As previously mentioned, this is how the solid-state power controller protects the wiring and components of an electrical system. Note that when actually implemented, this curve is defined as a range with upper and lower limits in order to eliminate continuous on/off switching due to the possibility of unsteady current during operation [14,24,47,48].

Understanding the i^2t profile is important in designing the behavior requirements of a solid-state power controller. The cables and wiring in the system also

follow similar curves, so the SSPC should be designed with lower limits than those components in order to ensure their protection in the event of a fault current [24]. A more detailed discussion of a general i^2t profile is provided as follows.

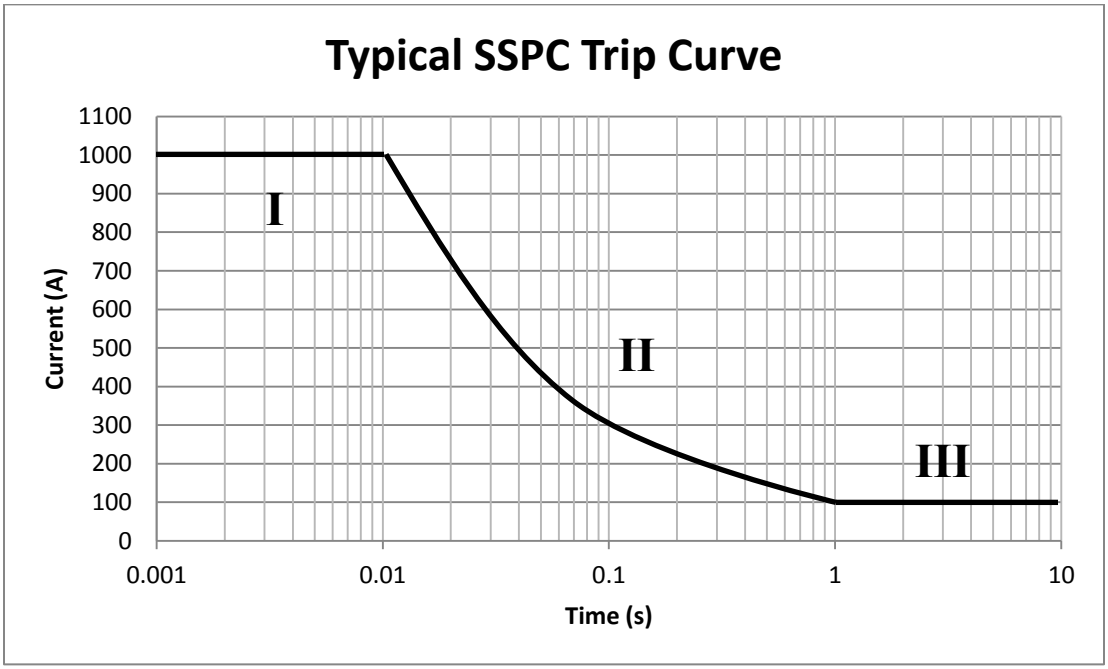

Figure 2.3. Example i^2t Trip Curve

As one can see in the figure, the curve is separated into three parts:

Part I: The first section of the curve represents the conditions where the input current is at the maximum fault rating (1000A in this example), resulting in an "instant trip". The time at the beginning of this section is determined by the minimum tripping time ability of the device, which is an inherit capability of the device and does not depend on the packaging. The horizontal length of this section directly corresponds to the "sustaining time" of the semiconductor, which for a given current input is the amount of time the device can operate for before it reaches the maximum allowable temperature, or junction temperature. The example curve shown above demonstrates

a sustaining time of 10 milliseconds at a fault current that is 10 times the nominal current rating. Because the sustaining time of the device is based on how much heat is produced and accumulated within it, this capability is heavily dependent upon the packaging of the module and its ability to efficiently draw heat away from the semiconductor. It is important to design the module so that the sustaining time of the semiconductor is as long as possible in order to reduce the likelihood of a pre-mature trip [48].

Part II: The intermediate portion of the curve relates the tripping time to any current input that is between the maximum fault rating and nominal rating (100A in this example).

Part III: The last section of the curve represents steady-state conditions, where the amount of heat generated in the semiconductor is equal to the amount of heat being dissipated through the rest of the module. Although the main concern is on the behavior of the module due to the maximum fault current, it is very important to verify that the module is able to reach thermal equilibrium and operate indefinitely at the nominal current rating.

While the i^2t profile is used to program the tripping characteristics of the power controller, this profile is directly dependent upon the ability of the module to manage the energy and heat that is generated during operation. The greatest amount of heat is generated when the current is at the maximum fault rating, so the work presented in this research focuses on the "instant trip" portion of the curve. The energy produced

within the semiconductor at any time during operation can be found according to the relation i^2Rt (units are in [J]), where R is the effective on-state resistance of the MOSFET. As a given current is applied over time, the device will absorb more energy and generate heat due to an effect called Joule Heating.

2.3.2. Joule Heating

Joule heating is the manner in which heat is produced in a conductor due to the passage of an electric current through it. As a given current passes through the conductor (or semiconductor in our case), power is dissipated according to the relation i^2R (units are in [J/s] or [W]). On an atomic scale, this phenomenon is explained as a result of the interaction between the electrons of the current and the ions that are present in the conductor. As the electrons in a flowing current collide with the ions of the conductor, energy is released in the form of heat and results in a temperature rise in the conductor. This heating effect caused by energy dissipation is often referred to as resistive losses and is usually an unwanted side effect of electrical systems. This undesirable heating forces current limitations in many applications, and is an essential concern in the proposed power controller.

Because the switches are only able to operate up to a specified junction temperature, it is important to limit the effects of joule heating in order to allow the devices to operate for as long as possible before reaching this junction temperature. Considering that the proposed module is designed to operate at the highest of current densities, the ability to mitigate the temperature rise in the semiconductors due to

these heating effects is of the utmost importance. The use of a SiC semiconductor and the aluminum-based packaging help to draw the generated heat away from the active region of the device, therefore reducing the rate at which the temperature rises within the device itself.

3. Modeling Considerations

Previous work in the development of this module has focused on the optimal spacing and density of dies per module [24,47-49]. Through iterative testing, this previous work showed that the optimum die layout consists of four evenly spaced dies. Using a lower applied current in order to study steady-state conditions, the previous work showed that a spacing of 6mm between any two adjacent dies achieves the lowest possible thermal impedance. If the dies are positioned any closer to one another, the heat flow away from one die becomes impeded by the flow away from the adjacent dies. When the dies are placed any more than 6mm apart the heat flow away from each die becomes impeded by the protruding walls of the baseplate [47,49]. The results of this research build off of these previous studies and do not include any further packaging concerns in relation to the placement of the dies.

It is important to note that although the heating in the module is a result of the electro-thermal effect known as joule heating, the simulations do not necessarily need to include any electrical components. Finite element analysis tools such ANSYS and COMSOL Multiphysics can solve for thermal effects based on electrical inputs, but because the correlation between input current and heat generation is known, this relationship can be used to directly apply inputs as thermal quantities. This reduces the computational effort required by the FEA software because the simulations are then

solving for one less dependent variable (voltage). As long as the relationship between temperature and on-state resistance of the MOSFET is explicitly known, it can be used to define the heat generation according to the i^2R relation.

As previously stated, one of the major considerations in the simulations of the module was to properly capture the dynamics of the joule heating (i^2R) in the semiconductor. The effective on-state resistance of the SiC MOSFET changes according to temperature, therefore introducing an important non-linear element into the model. As the device is active and current is flowing there is an initial heat generation related by i^2R to the on-state resistance of the MOSFET at the initial temperature. As heat is produced and absorbed by the device, the effective on-state resistance increases, which in turn increases the amount of heat generation, and in turn the on-state resistance of the device increases further. In order to properly document the behavior of the SSPC, this thermal runaway effect needs to be accurately represented in the simulations.

3.1. Dynamics of Non-Linearly Temperature-Dependent Resistance

In an attempt to include the non-linear behavior of the semiconductor resistance, previous work by DensePower divided the transient simulations by pre-determined time steps and performed each step individually [24,47-49]. During these simulations, the maximum temperature was evaluated before each step and the value of the resistance in the semiconductor was adjusted according the known relationship. While this process may be sufficient for the modules consisting of smaller dies (4.1mm x 4.1mm) where the resistance changes only about 100% across the operating

temperature range, this procedure is inadequate for the module in this research consisting of larger dies (7mm x 8mm) because the resistance changes by over 200% across this same temperature range. This extreme non-linearity of the on-state resistance requires a much greater number of time-steps/iterations to truly capture the dynamics of this non-linear heating effect, and manually performing enough of these steps to achieve credible results would be extremely time-consuming and inefficient.

For the simulation work in this research, the effects of this non-linearly varying parameter have been incorporated in a way so that the material property can be automatically reevaluated and updated by the software as often as is necessary for accurate results. This method is described as follows.

Manufacturer data provided resistance values for temperatures up to 200°C, but the module is designed to operate up to 350°C so the given data was first extrapolated out to the needed temperature range. Future work would require actual experimental data in the higher temperature range for even better accuracy. A second order polynomial was fit to the data to obtain an explicit relationship between temperature and on-state resistance; the full equation can be seen below in Equation 3.1 followed by the plot of on-state resistance vs. temperature in Figure 3.1. A second-order function was used as it sufficiently describes the behavior of the on-state resistance and does not create too heavy of a computational burden. This equation for resistance could be used to define the heat generation function in the model according to the joule heating relation i^2R (where i is current and R is resistance, units are in [J/s] or [W]). The 7 mm x

8 mm semiconductors have an active area of 46 mm^2 and the current is assumed to pass through the top 20% of each device, giving an active volume of 3.68 mm^3. After finding the active volume of the MOSFET, the above function was applied to the model as a heat generation load (in units of [W/m^3]). The transient simulations could be run by simply telling the program how many time steps/intervals to break the simulation into, and the re-evaluating and updating of the on-state resistance is automatically performed by the program as needed. Note that while most of this work is presented according to the Celsius temperature scale, the units of temperature in Equation 3.1 are in Kelvin, the standard unit of temperature recognized by the simulation software.

$$R_{ds-on}(T) = \left(7E-07 \times T^2\right) - \left(0.0004 \times T\right) + 0.0821 \quad [\Omega] \qquad \text{Equation 3.1}$$

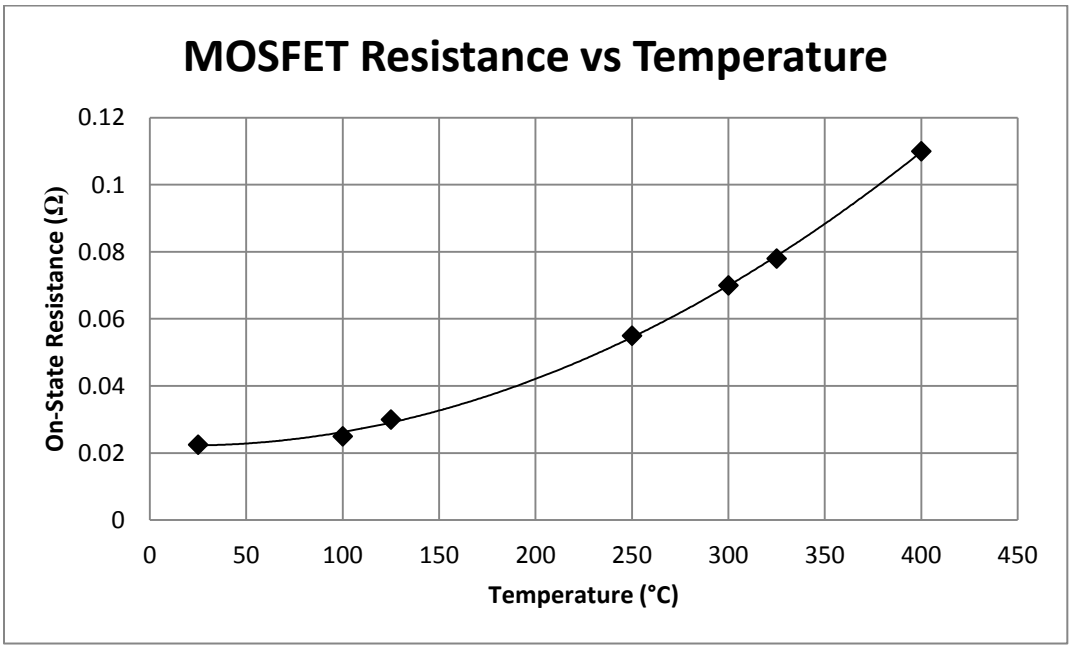

Figure 3.1. On-State Resistance of SiC MOSFETs vs Temperature

3.2. Choice of Simulation Software

Although both ANSYS and COMSOL Multiphysics were utilized to simulate and study the behavior of this module, the results presented here are produced solely from COMSOL. Efforts were switched exclusively to this FEA program based on previous work with the software, where it was found that the program was better suited and more user-friendly when using variable-dependent properties and loads. While both of these programs allow for this, COMSOL is built on the premise of solving multi-field problems and allows for direct input of any variable-dependent load while ANSYS requires several extra steps in order to define these types of loads. Also compared to COMSOL, ANSYS has limited capabilities when it comes to defining and evaluating variable-dependent material properties. COMSOL is also better suited for presentation of results as it allows for more control over plots and other graphical representations. For assurance before completely moving to COMSOL Multiphysics, both programs were run with identical parameters and it was found that both programs produced results that were within 2% of one another. Given the extreme non-linearity of the problem, this result was deemed acceptable. Therefore, please note that all future modeling and simulation considerations are in reference to the COMSOL Multiphysics software package.

4. Thermal Simulation and Characterization of Module

4.1. Setting up the Thermal Model

The overall geometry of the module is not complicated and was easily built by adding and overlapping volumes. With the model built, the material properties and loads/conditions could be applied to properly set up the simulations. In contrast to the heat generation load previously mentioned, the initial conditions and constraints on the model are very simple. An initial condition of 105°C was applied to all domains of the model, and to allow for thermal equilibrium a thermal ground of 105°C was applied to the entire bottom surface of the baseplate, which is where the module would be in contact with outside components when bolted into place. All of the simulations performed as part of this research assume adiabatic conditions where heat is only transferred by conduction through the module layers. The simulations also assume that all module layers have even surfaces and the effects of imperfect bonds are not considered. Also note that all of the simulations assume equal power density amongst the dies operating in parallel.

As previously mentioned, the loading in the simulations is a temperature-dependent heat generation following the form of i^2R, where i is the input current and R is the temperature-dependent resistance of the semiconductor device. Using the

resistance versus temperature function given above in Equation 3.1, the entire heat generation function (for the maximum fault current load of $240A_{DC}$ per die) is given below in Equation 4.1. In the semiconductor layer of the model, a separate volume was created inside of each device so that this load could be applied to only the active volume of each device. Again, please note that the unit of temperature used in Equation 4.1 is Kelvin.

$$Heatgen(T) = \frac{(240)^2\left(\left(6E-07\times T^2\right)-\left(0.0003\times T\right)+0.0732\right)}{3.68} \quad \left[\frac{W}{m^3}\right] \qquad \text{Equation 4.1}$$

With all of the loads and constraints set up in the model, the material properties could be applied to each respective layer. The material properties and thickness of each layer can be found below in Table 4.1. As seen in the table, the thermal conductivity of the SiC devices is given as a range because this property changes considerably over the operating temperature range of the module. While other properties may also be dependent upon temperature, none of these relations are as pronounced as that of the SiC thermal conductivity. Also, because this is the layer where all of the heat is generated it is also the most important layer to accurately represent in the model. In addition, this relation is best represented by a second-order polynomial which places a considerable burden upon the computational effort needed, and limiting the number of variable-dependent material properties helps keep this computational burden to a minimum. This equation describing the non-linear behavior of the SiC thermal conductivity is given below in Equation 4.2, along with Figure 4.1 which visually

demonstrates the relationship between thermal conductivity and temperature. Note that the units of temperature in the equation are again given in Kelvin.

	4H SiC	Silver Glass	Al trace	AlN	Baseplate
Density (g/cm^3)	3.21	7.52	2.7	3.3	2.4
Thermal Conductivity (W/m*K)	490-160	200	250	180	X - 230 Y - 230 Z - 120
Specific Heat (J/kg*K)	690	310	230	740	852
Thickness (mm)	0.4	0.08	0.381	0.635	6.35

Table 4.1. Thermal Properties and Thicknesses of Module Layers

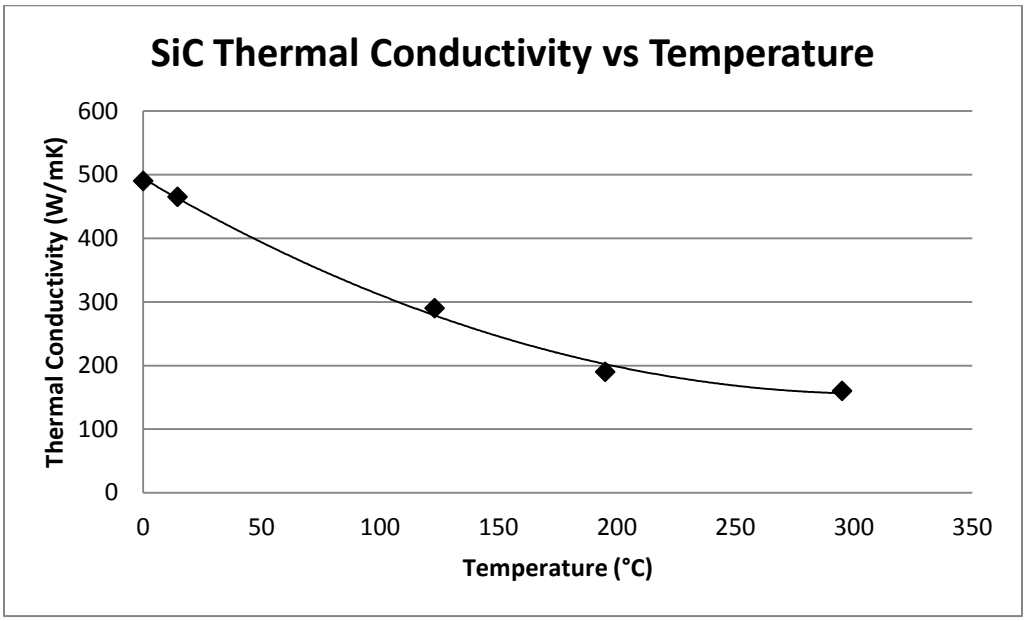

Figure 4.1. Thermal Conductivity of MOSFETs vs Temperature

$$k(T) = \left(0.0035 \times T^2\right) - \left(4.1 \times T\right) + 1351.4 \quad \left[\frac{W}{mK}\right] \qquad \text{Equation 4.2}$$

4.2. Steady-State Thermal Response

With the non-linear heating effect properly represented in the model, simulations could then be performed to investigate the thermal and mechanical behavior of the module during operation. Although we are interested in the transient behavior of the module in response to the maximum fault current, it was important to first verify that the module could operate indefinitely at the nominal current, meaning that the module could reach thermal equilibrium with a maximum temperature under that of the junction temperature so that there would be no chance of tripping under these conditions. To accomplish this, a steady-state simulation was run where the i^2R relation was applied to each of the MOSFETs in the model with a nominal current value of 24A (96A distributed evenly across all 4 dies). The results of this simulation are provided below in Figures 4.2-4.4.

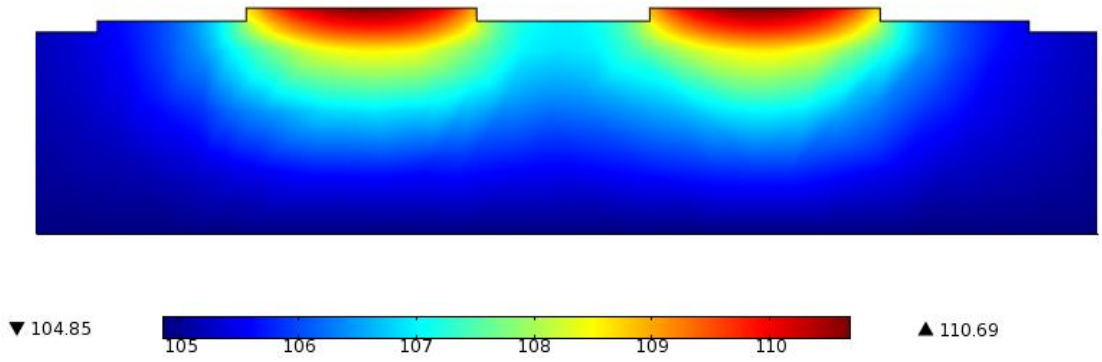

Figure 4.2. Steady State Cross-Sectional Temperature Distribution

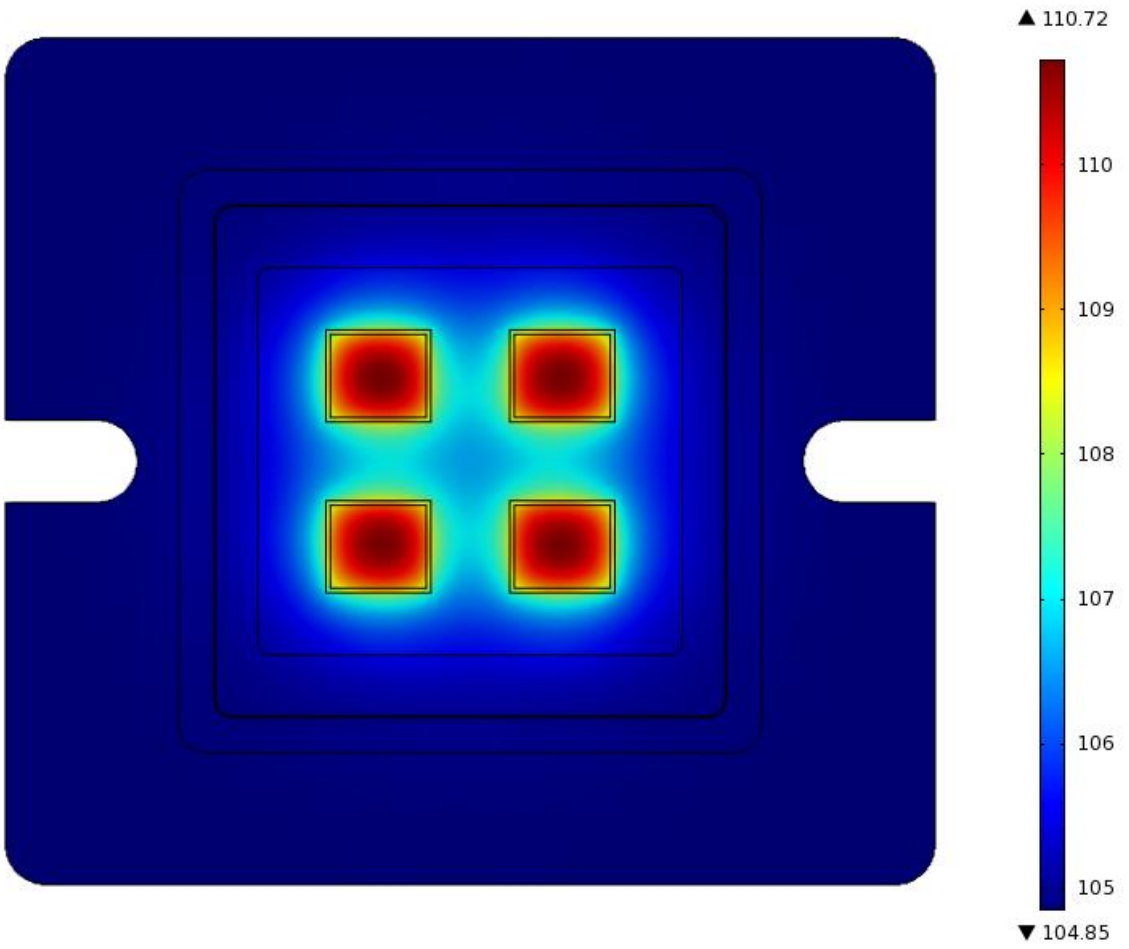

Figure 4.3. Steady State Surface Temperature Distribution

As seen in the above figures, the module reaches a peak temperature of approximately 111°C, a 6°C temperature rise. Naturally, the temperature is greatest in the semiconductor where the heat is generated and gradually varies down to the ambient temperature at the bottom of the baseplate which acts as a thermal ground in the module. Due to the near-uniformity of the thermal conductivity of the layers the temperature gradient is very even throughout the entire thickness of the module. A quarter-symmetry surface temperature plot is also provided below in Figure 4.4 to demonstrate how the temperature distribution is uniform in both the x and y-directions.

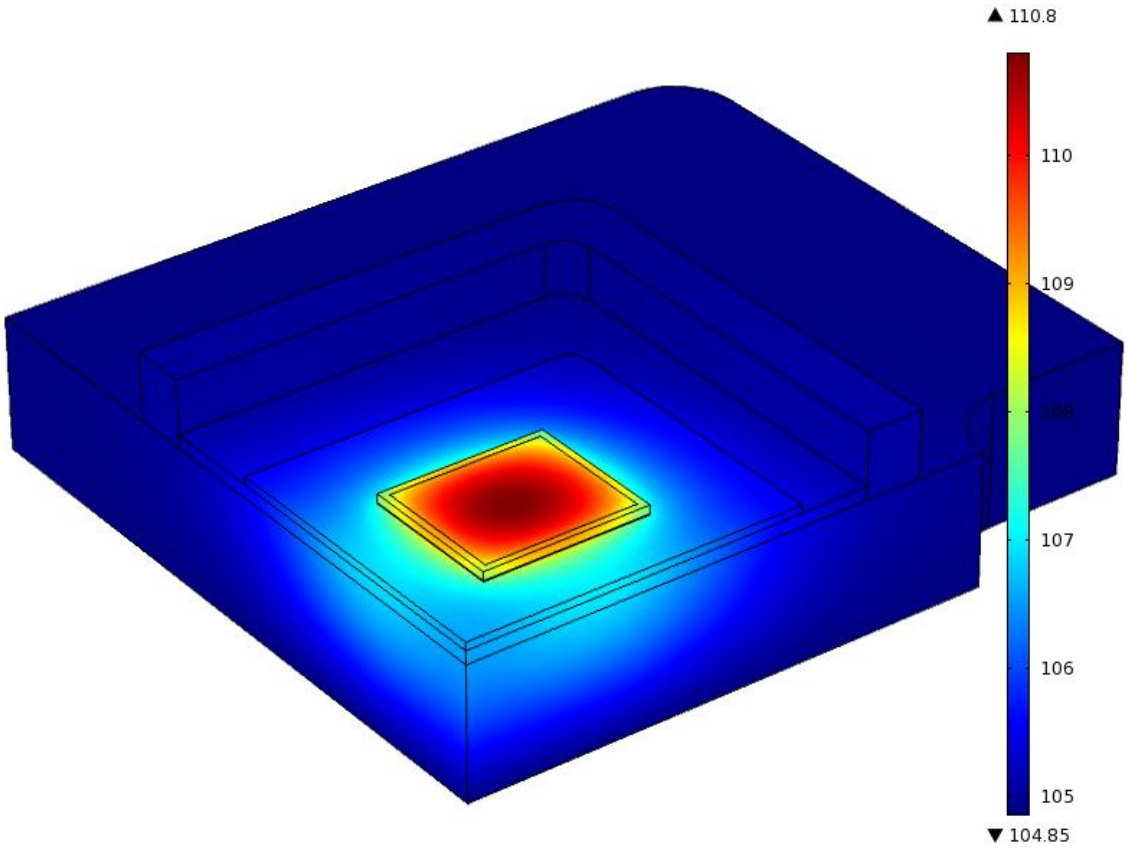

Figure 4.4. Steady State Quarter-Symmetry Surface Temperature Distribution

4.3. Transient Thermal Response

After demonstrating that the module is capable of operating indefinitely at the nominal current, it was time to study the transient behavior of the module in response to the maximum fault current of $960A_{DC}$. The i^2R relation was again applied to each MOSFET with a current value of $240A_{DC}$ ($960A_{DC}$ evenly applied across four dies) and the simulation was run for a pre-determined length of time. This run time was initially estimated based upon the results of previous work with the smaller dies. Once a simulation finished, the results could be post-processed to find the maximum temperature at the end of the running time. Based on this result, the simulation was

run again with a better-estimated run time. This semi-guessing strategy was necessary due to the lack of a temperature-based cutoff option in the software. After several runs it was found that the module is capable of sustaining a maximum fault current rating of $960A_{DC}$ for approximately 3ms before reaching the maximum junction temperature of 350°C. A surface temperature plot of the entire module is provided below in Figure 4.5.

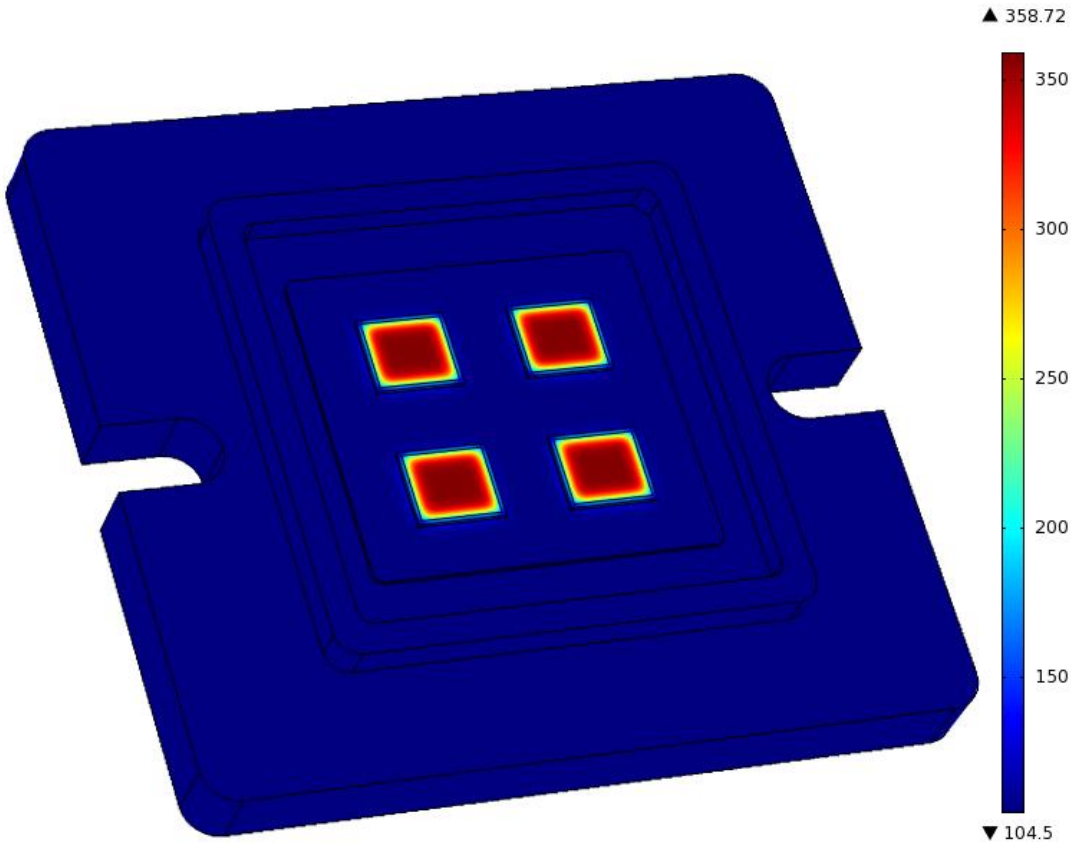

Figure 4.5. Transient Surface Temperature Distribution

With the sustaining time determined, it is possible to calculate the i^2t constant for the trip profile of this specific solid-state power controller. Multiplying the sustaining time by the square of the fault current per die, it is found that the semiconductors have a trip constant of 172.8, which is over 4 times greater than the constant determined for the DensePower module consisting of smaller (4.1mm x

4.1mm) dies [49]. The extreme improvement in this parameter helps demonstrate the impressive power and heat management capabilities of the module.

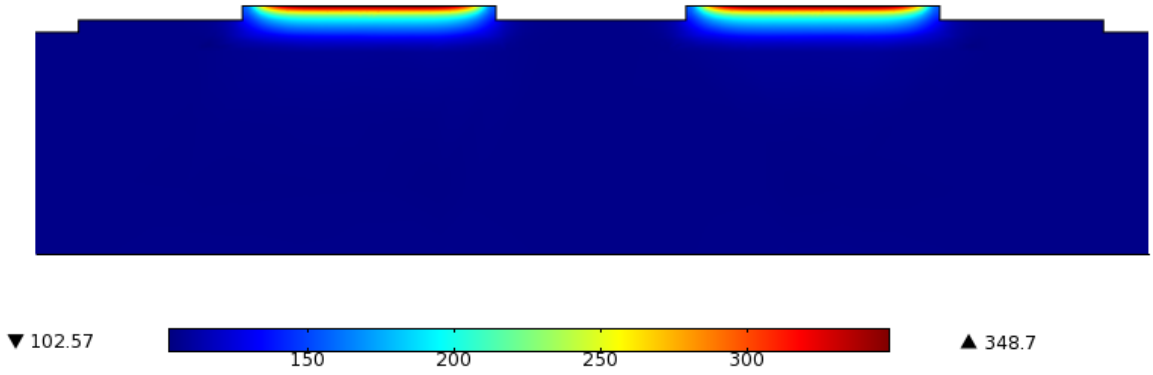

Figure 4.6. Transient Cross-Sectional Temperature Distribution

In the time it takes the MOSFET to reach the junction temperature the produced heat is only able to diffuse down through the module just slightly into the baseplate, but again the temperature gradient produced is very uniform as seen above in the cross section provided in Figure 4.6 or in the close-up provided below in Figure 4.7. This even distribution of temperature demonstrates that the generated heat is evenly spreading through the layers, again due to the near uniformity of thermal conductivity of the layers. These visuals help demonstrate the overall thermal behavior of the module, but do little to truly illustrate the capabilities of the module. In order to better demonstrate the thermal management capabilities of the power controller, it is necessary to quantify the amount of generated heat that is dissipated through the module.

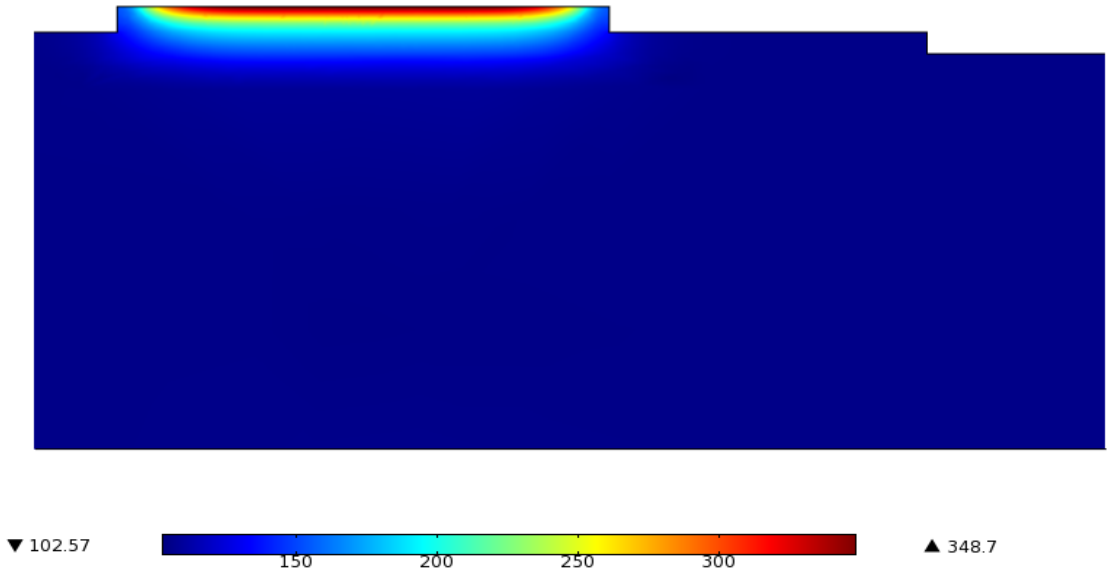

Figure 4.7. Transient Cross-Sectional Temperature Distribution Close-Up

4.3.1. Thermal Characterization Through Energy

To determine how much heat is dissipated through the module, it was necessary to first determine how much energy the MOSFETs produce during operation to the junction temperature. Quantifying the produced energy began with the energy relation i^2Rt (where i is current, R is resistance, and t is time). The fault current is known to be $240A_{DC}$ (in each device), and from the results of the simulations the operating time to junction temperature at this current is known to be 3ms. Even with this information, the amount of produced energy cannot be easily determined because the on-state resistance of the MOSFET changes during operation. If the behavior of the device's resistance was known as a function of time then the energy could be solved for by multiplying this function by the current-squared and then integrated over the known

operating time range (0-3ms), as shown below in Equation 4.3. Unfortunately, the behavior of the resistance is only known as a function of temperature, so it was necessary to find a way to define the resistance as a function of time.

$$E = \int i^2 R(T) dt \quad [J] \qquad \text{Equation 4.3}$$

To ultimately relate the resistance to time, ax explicit relationship was found between temperature and time and then inserted into the equation relating resistance to temperature. This relationship between time and temperature was found by utilizing probes in the simulation software. A probe was placed directly in the middle of the active volume of the MOSFET and recorded the temperature at that point several times throughout the simulation. This data was plotted and fit with a third order polynomial in order to find the explicit relationship between temperature and time. This plot is provided below in Figure 4.8, followed by the relation in Equation 4.4. Note that in the equation, the units of time are in seconds and the units of the temperature produced are in Kelvin.

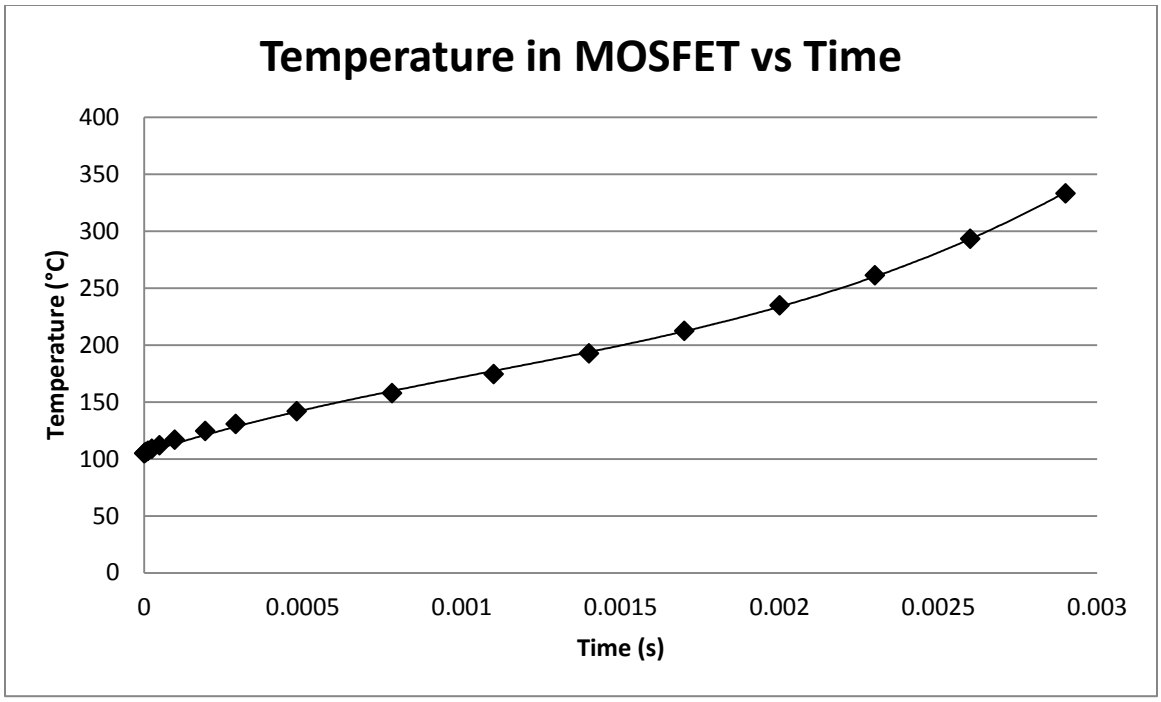

Figure 4.8. MOSFET Active Volume Temperature vs Time

$$T(t) = \left(1E10 \times t^3\right) - \left(3E7 \times t^2\right) + \left(88300 \times t\right) + 378 \quad [K]$$ Equation 4.4

Although plugging Equation 4.4 into Equation 3.1 for every temperature variable produces a very complex function, it can be easily handled through the use of computing tools such as MATLAB. This newly formed equation was integrated according to Equation 4.5 below and then multiplied by the squared value of the fault current. Performing the integration with the software, it was found that 9.846 joules are produced by each semiconductor during the sustaining time of 3ms. Note that this is the energy produced in only one device, so the entire module is able to absorb approximately 40 joules before reaching the junction temperature.

$$E = \int_0^{.003} (240)^2 R(t) dt \quad [J]$$

Equation 4.5

Although approximately 40 joules are produced in the MOSFETs during operation at the maximum fault current, not all of this energy is absorbed by the devices. One of the primary concerns of the SSPC was the rapid accumulation of heat in the semiconductors, so the materials used for the power switches as well as the packaging were chosen primarily based on their ability to draw heat away from the active volume of the semiconductors (by means of a high thermal conductivity). In order to assess the efficiency of the overall package, it was necessary to compare the amount of produced energy to the amount of energy that is actually absorbed by the MOSFETs.

Determination of the amount of energy absorbed by the semiconductors during operation under the maximum fault current was a simple process. Because the material properties and change in temperature of the active volume of the MOSFETs is known, and because heat is a form energy, the amount of energy absorbed could be calculated according to Equation 4.6 below (where Q is heat, m is mass, c_p is specific heat, and ΔT is change in temperature). The amount of heat (or energy) absorbed within the active volume of one semiconductor while operating from ambient to junction temperature is found to be 1.997 joules. Therefore, the total of active volumes in the module absorbs approximately 8 joules during operation to junction temperature.

$$Q = mc_p \Delta T \quad [J]$$

Equation 4.6

Comparing the amount of energy produced to the amount of energy absorbed, it is seen that only about a fifth of the energy produced due to resistive losses stays within the active volume of the MOSFETs while approximately 80% of this generated heat is spread through the rest of the semiconductor and the module. This demonstrates that a low overall thermal resistance has been achieved with the design that produces efficient thermal management in the module. These results substantiate the use of a SiC-based semiconductor and the aluminum-based packaging as a means of providing the thermal management capabilities necessary for operation at the proposed current density and temperature range.

5. Mechanical Simulation and Characterization of Module

5.1. Setting up the Thermal Stress Model

Using the information from the thermal analysis and including the mechanical material properties, the program is also able to simultaneously solve for the stresses in the module due to the heating up and expansion of the layers. In the thermal stress simulations, all of the thermal loads and conditions were kept the same as before and the only new condition was that of a zero-displacement condition that was applied to the bottom surface of the baseplate. Now that the program was being asked to solve for extra parameters, note that quarter-symmetry was implemented in these simulations to reduce the computational burden and accelerate the simulations. The mechanical properties of each of the module layers are provided below in Table 5.1.

	4H SiC	Silver Glass	Al trace	AlN	Baseplate
Young's Modulus (GPa)	410	11.1-3.0	70-50	330	98.6
Poisson's Ratio	0.14	0.33	0.35	0.24	0.30
Coefficient of Thermal Expansion (ppm/°C)	4	16	23	4.5	X - 4 Y - 4 Z - 24

Table 5.1. Mechanical Properties of Module Layers

Note that the Young's modulus of two of the layers – the silver glass adhesive and the aluminum trace – are given as a range. This is because it was found that these properties change considerably over the operating temperature range.

While the relevant material property data for aluminum could only be found for temperatures up to 200°C, extrapolating this data out to 350°C indicates that the Young's modulus of this layer will lower by approximately 20% over the operating temperature range of the module. This demonstrates that the aluminum becomes significantly softer as temperature increases in response to a fault current. This is beneficial to the module for it will mitigate the accumulation of stresses in this layer and therefore it is important to include this material behavior in the simulations. A plot demonstrating the relation between temperature and Young's modulus of aluminum is provided below in Figure 5.1. This behavior can be closely approximated by a linear relation as presented below in Equation 5.1. Note that this equation uses temperature units in Kelvin to produce a Young's modulus in Pascal so that it may be used in the simulation software.

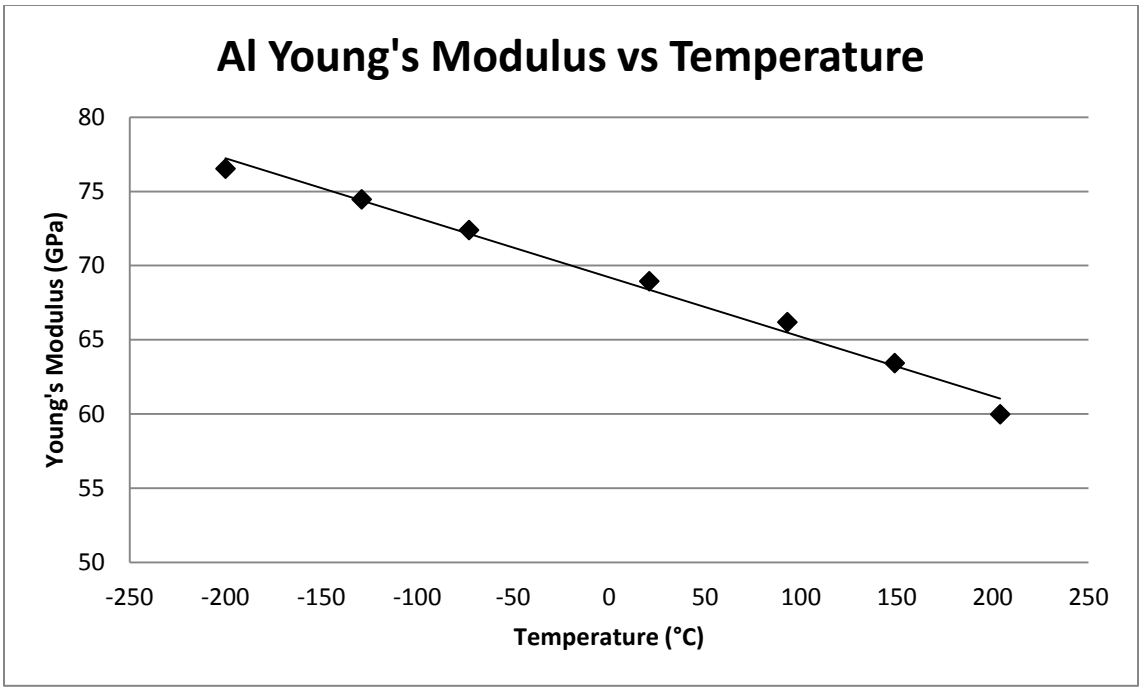

Figure 5.1. Young's Modulus of Aluminum vs Temperature

$$E(T) = -4E7 \times T + 8E10 \quad [Pa]$$ Equation 5.1

The same could be said for including the temperature dependent Young's modulus of the silver glass layer, but this material's behavior is a bit more complicated. This is because the silver glass adhesive becomes much softer at higher temperatures and actually undergoes a glass transition at approximately 170°C. At this temperature, the material enters a more rubber-like state and its Young's modulus significantly and rapidly decreases with further heating. The relationship between the Young's modulus of the silver glass and temperature was provided directly by the manufacturer and is presented below in Figure 5.2. As seen from the figure, the behavior of this property can be described as a fairly linear section followed by a non-linear section, therefore

making it difficult to define the entire relation with a single equation unless it is of very high-order. The use of a higher-order polynomial may still not sufficiently describe the behavior of the layer, and applying such an equation in the program would definitely add a significant computational burden to the simulations. In order to circumvent this problem an alternative technique was used in order to capture the dynamics of the silver glass behavior. Using data from the manufacturer, an extrapolation function was created where lower-order equations could be used to find the value of Young's modulus at any temperature. This allows us to incorporate the overall non-linear behavior in a way that will not overburden the available computing resources.

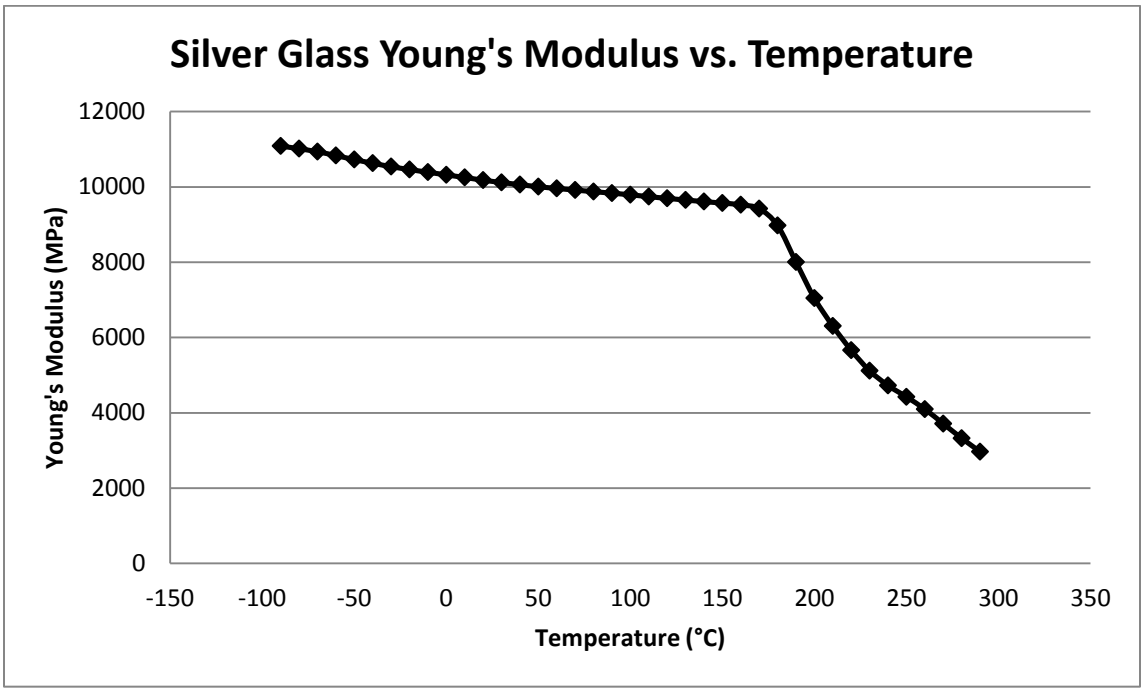

Figure 5.2. Young's Modulus of Silver Glass vs Temperature

5.2. Transient Response

Figure 5.3 below shows the stress tensor in the x-direction at 3ms. As indicated by the legend, most of the module is experiencing compressive stresses. This may be alarming at first due to the general understanding that materials tend to expand as they heat up, but this is actually why the module is experiencing compression. The most important parameter in the module is the coefficient of thermal expansion as it is directly responsible for the behavior of the module layers. To understand the behavior of the module layers one could look, for example, at the AlN layer and those adjacent to it. From looking at Table 5.1 above, once can see the relation of the CTEs of the Al trace, ceramic AlN, and composite baseplate layers. Disregarding the z-direction CTE of the baseplate (these results are more focused on the interaction of the layers in the xy-plane), there is a reverse-hierarchy in this parameter from the baseplate up to the Al trace layer that causes the compression observed through the simulation results.

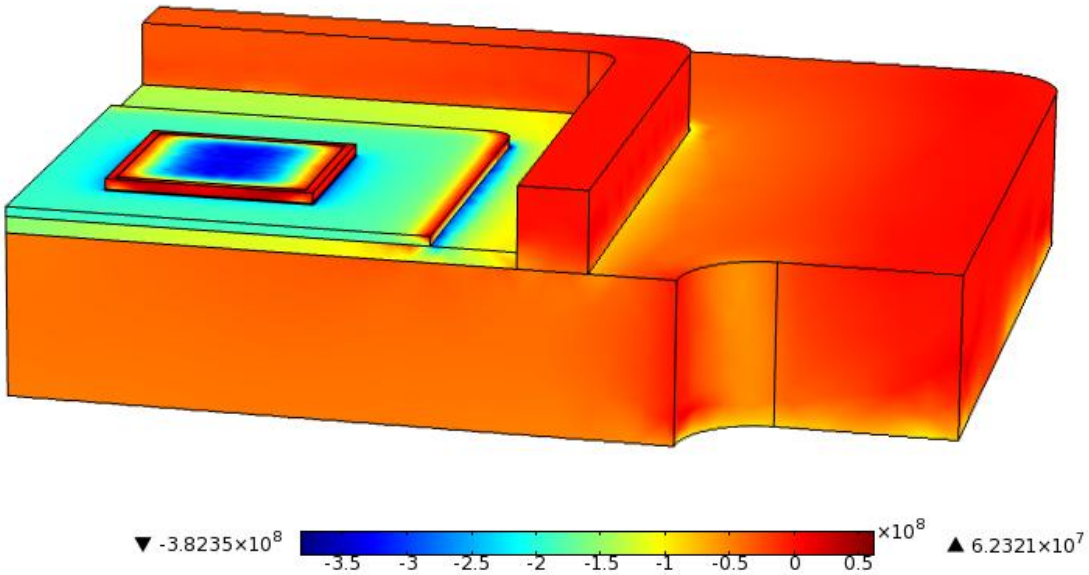

Figure 5.3. X-Tensor Stress Distribution at 3ms

Due to the temperature rise in the module, each of the layers wants to expand, and the amount of this expansion is determined by the thermal expansion coefficient of each layer. Because the baseplate has the lowest CTE, it naturally wants to expand less than the layers on top of it, so when the AlN layer tries to expand further (due to its higher CTE) its movement is limited by the baseplate with its lower CTE. The ceramic wants to expand, but because it is bonded directly to the baseplate its movement is restricted and therefore the layer experiences a compressive stress. The AlN also has the Al trace bonded directly to it, and the relatively much higher CTE of the Al trace makes it want to expand much more than any of the other layers in the module. This great urge to expand pulls outward in all directions on the top surface of the ceramic, resulting in a slight alleviation of stresses in the area where the two layers are connected, but also resulting in a greater compressive stress seen in the surrounding

areas of the ceramic. Figure 5.4 is provided below to provide a visual demonstration of how the module layers wish to expand. Note that the deformation in this figure is exaggerated by approximately 300 times.

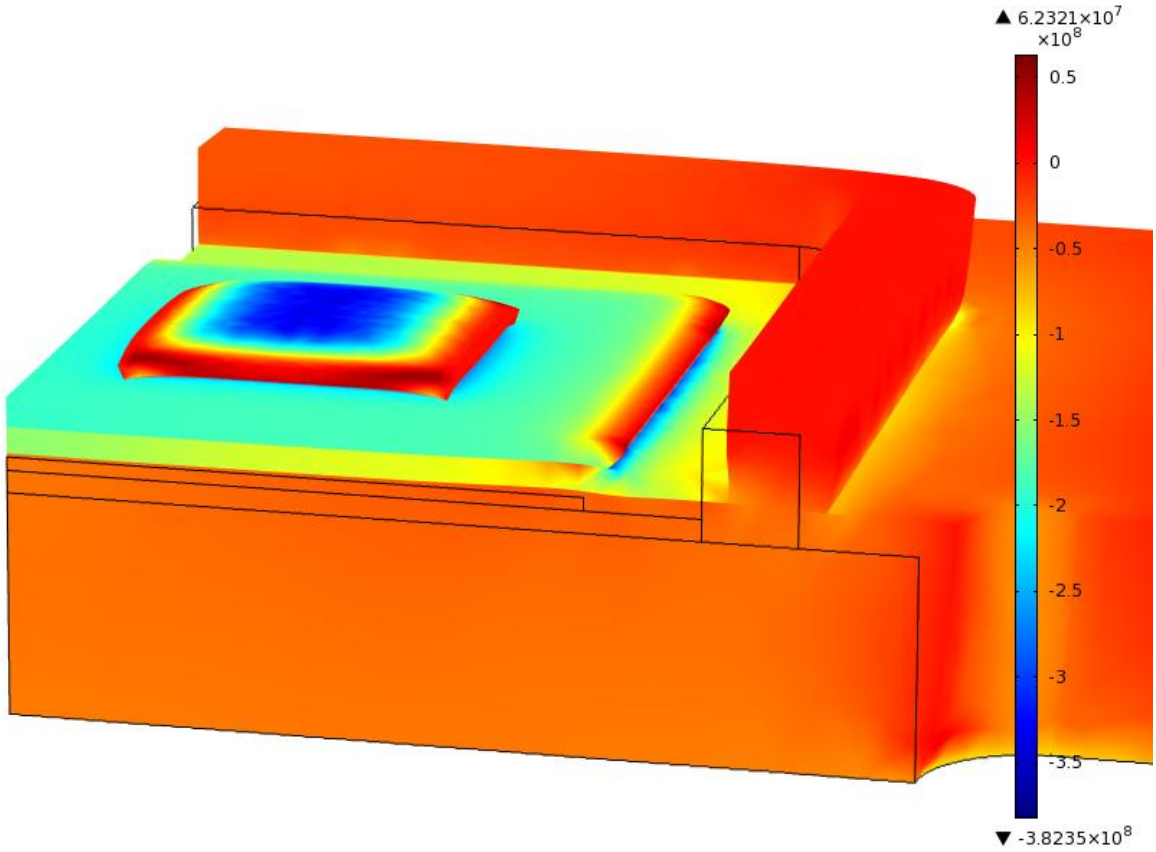

Figure 5.4. X-Tensor Stress Distribution Close-Up at 3ms (300x Deformation)

Figure 5.5 also demonstrates this behavior by providing a xy-plane cross-section through the top of the ceramic layer. Looking at the figure, once can easily discern the area where the Al trace layer is bonded to the ceramic by observing the sudden increase of compressive stresses. One can even make out the area where the die would be located in the stack-up. This is due to the interplay of the CTEs between the Al trace, die

attach adhesive, and the aluminum layers. The generated stresses between these layers are transferred down into the AlN ceramic layer.

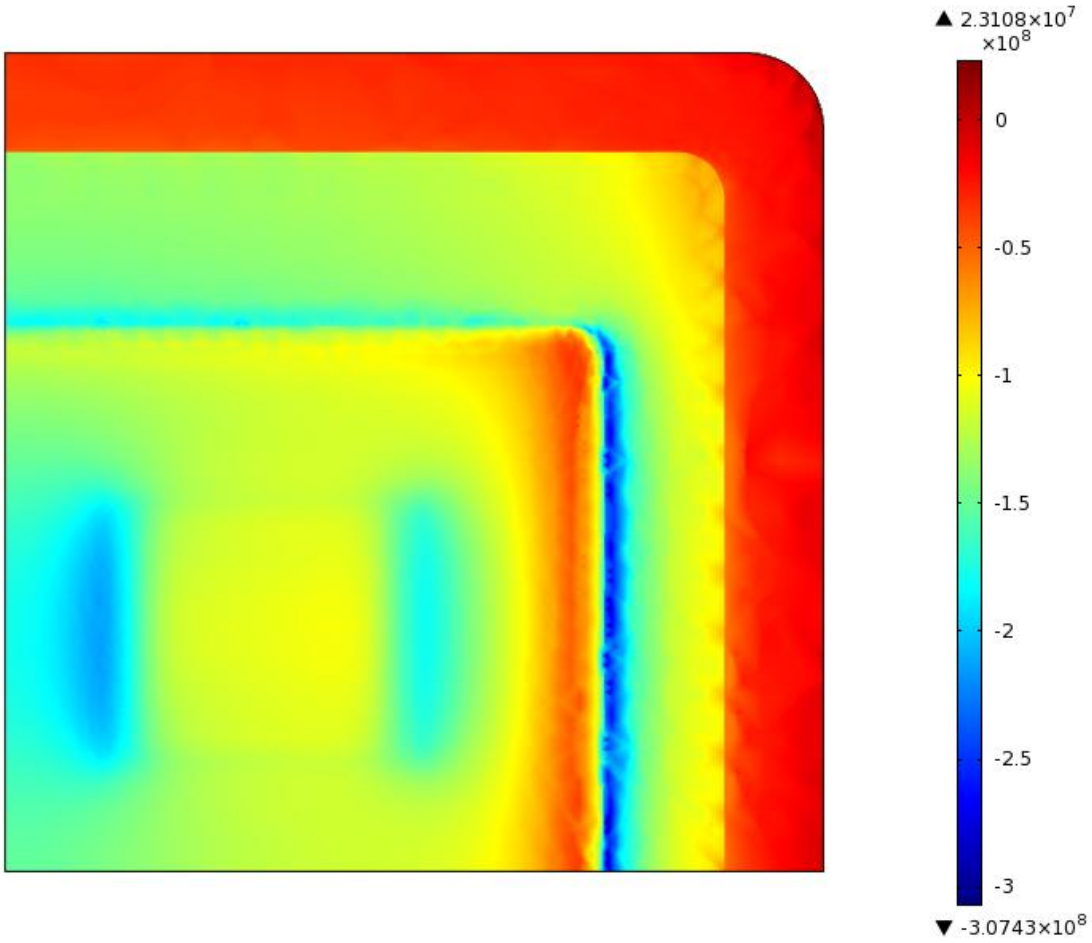

Figure 5.5. Cross-Sectional X-Tensor Stress Distribution Through AlN at 3ms

Although most of the module is in compression, some parts of the module are able to expand more and experience tensile stresses. The greatest tensile stress observed in the module is approximately 62 MPa and is observed in the Al trace layer and in the SiC MOSFETS. The Al exhibits this stress in its free edges where it's allowed to expand the most. In slightly different behavior, the MOSFETs experience this stress at the corners of the active region where the material wants to expand the most and is

causing the dies to want to bulge out, but by an amount that can only be observed through great magnification. These two materials have approximate tensile strengths of 248 MPa and 200 MPa, respectively, so each material has a factor of safety of at least three during this mode of operation. The baseplate is the only other layer to experience any tension, and experiences a maximum stress of about 10 MPa in the top portion of the protruding baseplate. The manufacturer of the baseplate states that it has a tensile strength of approximately 100 MPa, so it is also well under its limit due to the fault current conditions.

Although the tensile stresses experienced in the module are easily manageable, the majority of the module experiences compression and the magnitude of these stresses are considerably greater than their tensile counterparts. The greatest compression in the module is observed in the AlN ceramic at the boundary where it is bonded to the aluminum and has a magnitude of about 382 MPa, which is well under its compressive strength. The AlN can easily withstand these stresses, and this behavior was expected as ceramics always perform well under compression. Also, note that this stress is greater than the maximum compression seen in the cross-section provided above. This helps demonstrate the general trend that the greatest stresses – compressive or tensile – are observed near or at the surface where they are bonded to other layers. This further validates the role of the CTE mismatch between layers and how important it is to minimize this mismatch with proper material selection.

The next greatest compression observed in the module is approximately 360 MPa and is seen in the aluminum trace layer and the MOSFETs. The aluminum experiences this compression at the boundary where the MOSFETs are bonded to it, and even though the simulations take into account the softening of the aluminum, the stresses in this layer are still relatively close to its compressive strength of 530 MPa, resulting in a factor of safety of about only 1.5. The SiC dies experience their greatest compression in the center, but have a compressive strength that is even higher than the ceramic layer. To better see these stresses, especially those at the boundaries between layers, a close-up of the x-tensor stress distribution is provided below in Figure 5.6.

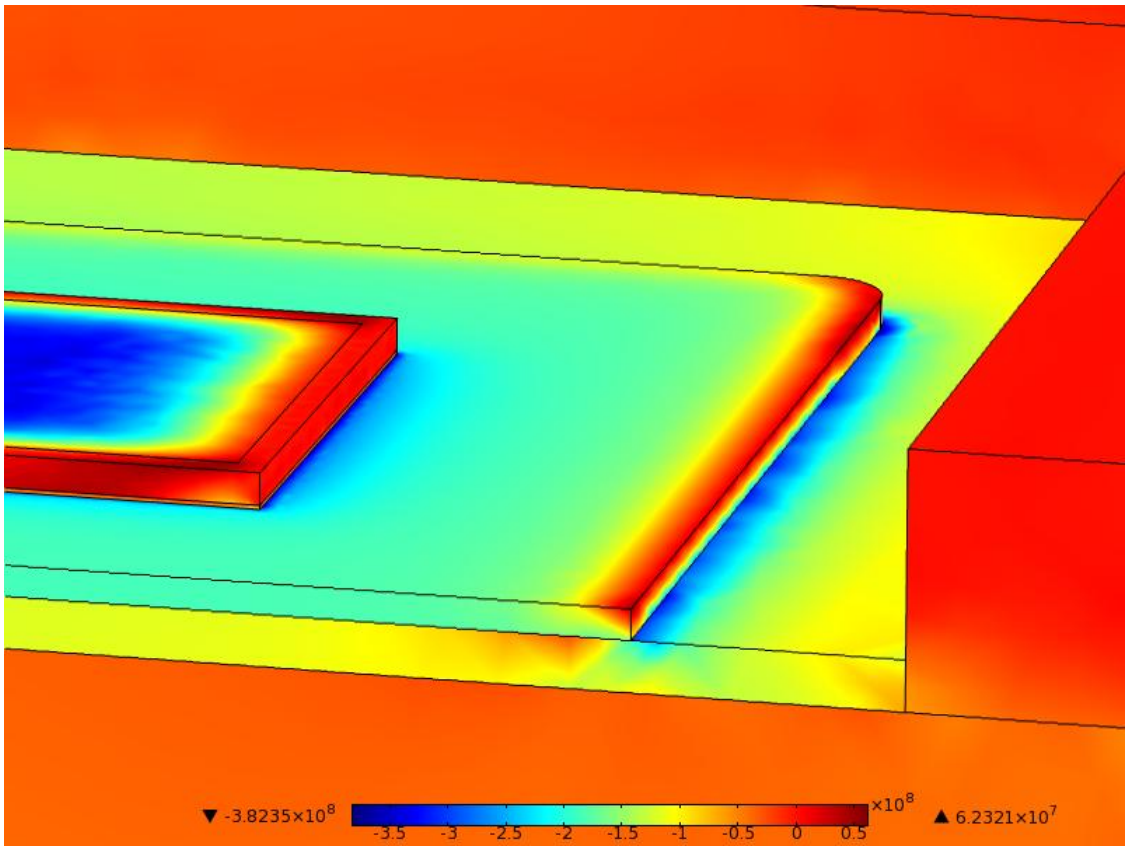

Figure 5.6. X-Tensor Stress Distribution Close-Up at 3ms

Unfortunately, the manufacturer of the silver glass adhesive could not provide stress limits for the material. The results of the simulation work do not bring up much concern for this layer, however, as the entire volume of the silver glass adhesive experiences a very uniform compressive stress of only about 60 MPa. Also, the manufacturer of the MMC baseplate could not provide any information on the compressive strength of its product, but like the silver glass, this layer experiences a small compressive stress of 60 MPa and does not cause much of a concern.

A summary of the stress results is provided below in Table 5.2. Although this discussion and the associated figures have focused on stresses in the x-direction, the stresses in other directions were studied as well and the results were congruent with what is seen in this direction. For example, the stress pattern in the y-direction looks identical to that in the x-direction but all of the stresses are lower than their respective stresses in the x-direction. Also note that the stresses documented in this research are determined through nodal averaging. Typically this technique is not fit for models with multiple materials, but this averaging in the model is only within domains and not across shared boundaries of dissimilar materials.

	Maximum Compression (MPa)	Material Strength (MPa)	Factor of Safety	Maximum Tension (MPa)	Material Strength (MPa)	Factor of Safety
4H SiC	360	3900	10.83	62	200	3.23
Silver Glass	60	-	-	N/A	-	-
Al trace	360	530	1.47	62	248	4.00
AlN	382	2000	5.24	N/A	270	-
Baseplate	60	-	-	10	103	10.30

Table 5.2. Stresses in Module Layers

5.3. Mesh Quality and Results Convergence

In order to provide confidence in the results from the simulations, a mesh convergence test was performed using the thermal stress results. An integral part of a finite element analysis is the mesh, the density of which determines how many elements or degrees-of-freedom (DOF) exist in the model and therefore how many equations must be simultaneously solved by the FEA software. Depending on the geometry and the available computing resources, it may be difficult to produce a mesh consisting of higher quality elements, but it is important to consider mesh quality as a poor mesh may produce results that are more dependent upon the mesh itself than the actual geometry, and in a case of extremely poor mesh quality the results may not converge at all. Mesh (or element) quality is presented by a percentage or a scale of zero to one, where a "perfect" element would have a quality of one or 100%. Although different metrics are used to determine the quality, it is always based on the shape of the elements and how close they are to the optimum shape for that particular type of element [58]. Often this deviation from the ideal shape is determined by looking at the interior angles of the element. For example, all of the interior angles of a quadrilateral element have an optimum value of 90°, forming a rectangle, while those of a triangular element should be as close as possible to 60°, forming an equilateral triangle. In order to provide confidence in the simulations, a mesh convergence test was performed using the thermal stress results.

The mesh convergence test was performed using the h-method, where mesh refinement is achieved by decreasing the size of the elements in the mode. This is in contrast to the p-method, where refinement of the mesh is performed by increasing the polynomial degree of the elements [58,59]. Initial simulations began with a very rough mesh consisting of approximately 21,000 elements. The overall mesh density was increased to consist of about 44,000 elements, and then the mesh was refined again to create a mesh consisting of approximately 83,000 elements. At this point, the results were found to be converging, but the mesh quality in the Al trace layer was still less than desirable, so the mesh in this region was refined again to create a model consisting of 96,000 elements. Figure 5.7 below shows the mesh quality of the model at this element count. Although the lowest quality of elements in the model is about 55%, the quality of these elements has been improved by about 400% from earlier meshes, and disregarding the silver glass layer the rest of the module is comprised of high quality elements generally exhibiting a quality of approximately 70% or greater.

Note that this low mesh quality is only observed in the silver glass die attach layer. The poor quality in the silver glass layer can be attributed to how thin this layer is in comparison to the rest of the module, which makes it difficult to properly mesh without drastically refining the mesh of the layers it is adjacent to, which would in turn vastly increase the computational burden of the simulations. The alternative to this poor mesh quality in the silver glass layer would be to completely remove this layer from the model and replace it with a “thermally resistive layer” boundary condition in the FEA software. This would eliminate the need to actually mesh this thin layer while

still accurately representing the thermal behavior of the module due to the physical presence of the layer. Unfortunately, however, this technique does not have a mechanical equivalent that would allow us to preserve the accurate mechanical behavior of the module so it was necessary to include this layer in the model despite the undesirable mesh quality that is generated in this section.

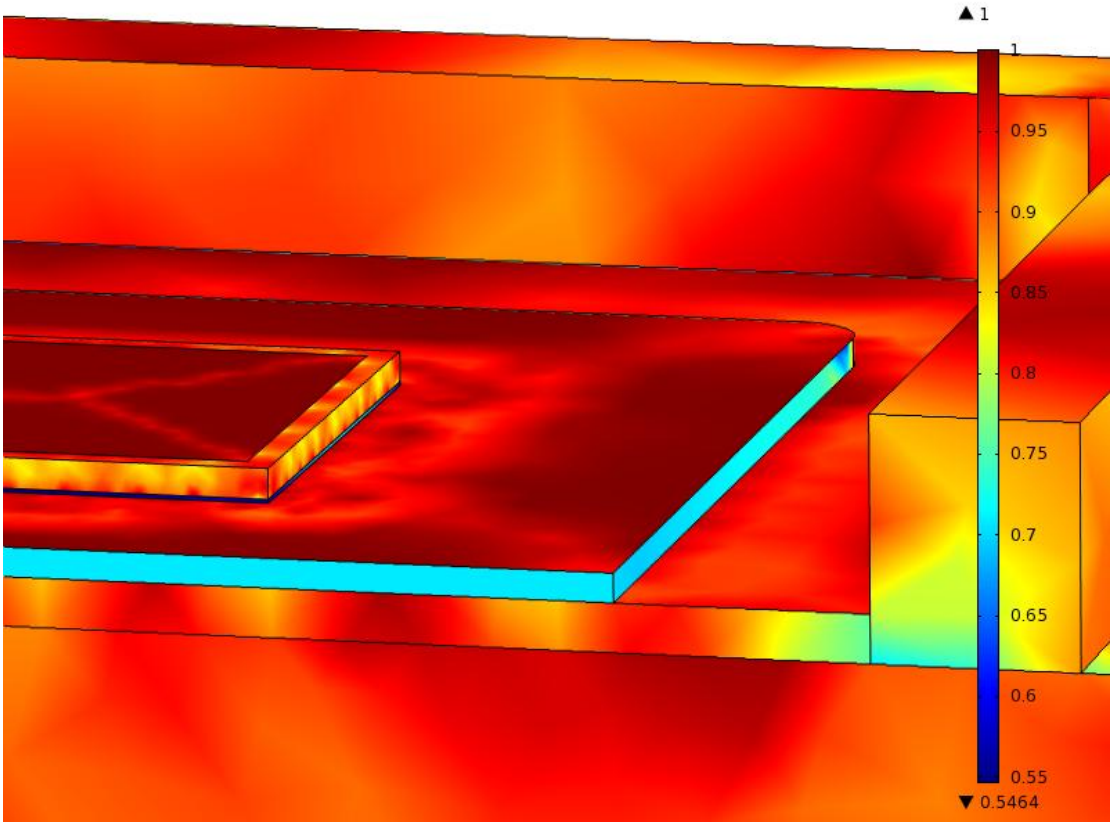

Figure 5.7. Mesh Quality Distribution for 96,000 Element Model

In addition to checking the quality of the mesh, the actual results of the thermal stress simulations were also checked for convergence. When checking for convergence of stresses, focus was on the compressive stresses that dominated the module. The tensile stresses observed during operation were so low in comparison to those of

compression that any change in the values would be a small percentile change and therefore would not give a good account of the convergence of the overall results. In the simulations with an element count of 44,000 the largest compressive stress seen in the module was 365 MPa, while at a count of 83,000 elements this value increased to 381 MPa. As stated before, this change in results was already proving convergence but the mesh was refined once again to produce a better mesh quality in the Al trace layer. The final model consisting of 96,000 elements produced a maximum compression of 382 MPa, which absolutely proves convergence with a percent change of less than one-half of one percent from the previous model. The results of this convergence test are summarized below in Table 5.3.

Element Count	Minimum Mesh Quality (Excluding Silver Glass layer)	Minimum Stress (MPa)	Stress Percent Difference
21,000	0.010	-351	-
44,000	0.108	-365	3.989
83,000	0.546	-381	4.384
96,000	0.680	-382	0.262

Table 5.3. Mesh and Results Convergence Results

5.4. Pre-Stress

Although the initial simulations showed that there is not failure in any of the layers during operation, these results did not include any previous stress state that may exist in the module. Stresses may be present in the module before it is ever put into operation due to the manufacturing process; these would be known as the pre-stresses. The first three layers of module – the baseplate, AlN ceramic, and Al trace – are first

fabricated together, and then the SiC semiconductor is attached using the silver glass epoxy. The first three layers are fired together at 700°C and then allowed to cool down to room temperature in approximately two to four hours.

To determine the stresses in the module due this fabrication process, a model was first built that included only the bottom three layers. Although these layers are fired at 700°C, they start to set during the cool down at approximately 660°C, so this was used as the starting temperature in the simulation. Convection was applied to all free surfaces of the module, and because the cool down time is given as a range of two to four hours, various convection coefficients were used in order to let the module layers cool down to room temperature in different lengths of time.

From post-processing these simulations it was seen that the plots of specific stress tensors corresponded identically to those from the previous simulations, but only differed in the magnitudes of the stresses. Tension was still observed in the free edges of the module while the greatest compression was seen in the boundary between the AlN ceramic and Al trace layers, but the values of these stresses are minimal compared to those that exist in the module during operation. The stresses observed in these simulations are so small in comparison to those seen during operation that the previous results can be considered valid and accurate. For example, the compressive stresses – which are the ones we are most concerned about during operation – resulting from the fabrication process are only a fraction of one percent of the stresses observed in the module during operation.

Through the use of different convection parameters, it was found that the stresses in these layers change only minimally according to the cooling rate. Therefore it can be said that the pre-stresses in the module do not have a strong second-order dependence upon the temperature change, but are more dependent upon the temperature change itself. Table 5.4 below summarizes these results by comparing the maximum and minimum stresses observed in the module due to different cooling rates.

Cooling Time (Hours)	Convection Coefficient (W/m^2K)	Maximum Stress (MPa)	Minimum Stress (MPa)	Final Temperature (°C)
2	5	1.000	-3.703	20.479
2.5	4	0.740	-3.655	20.479
4	2.5	0.713	-3.662	20.479

Table 5.4. Cool Down Times and Stresses

5.5. Harsh Environment

Although the simulations performed up until this point all considered that the module starts from an ambient 105°C, it is of great importance to study the behavior of the module when subjected to very low temperatures. The lower spectrum of general military aerospace applications reaches as low as -65°C, so simulations were performed to study the behavior of the module when subjected to very low ambient temperatures. This was done by setting the entire module to room temperature and applying convective boundary conditions on all free surfaces in order to allow the module to cool to the desired temperature. Thermal stress simulations were performed where the module was subjected to ambient temperatures as low as -65°C.

From observing the results of these simulations, it was found that the module has an inflection point at approximately room temperature. As temperatures drop below this point, the behavior of the module 'flips' from what it was due to heating. This is understandable as generally materials tend to shrink or contract as they drop in temperature. Also in contrast to the behavior due to previous conditions, most of the module is now experiencing tension, which is a result of the mismatch of thermal expansion coefficients of the layers. To help demonstrate the behavior of the module, a cross-section of the x-tensor stress distribution at -65°C through the AlN layer is provided below in Figure 5.8. Using the ceramic layer as an example once again, it can be understood by explaining that the contraction of the ceramic layer is limited by the baseplate because it has a lower CTE than the ceramic. Because it cannot contract as it would like to it experiences an initial tensile stress, and then the Al layer on top pulls inward with even greater force on the ceramic because it is attempting to contract much more due to its much higher CTE. This interplay of CTEs creates the tensile stress observed in the AlN.

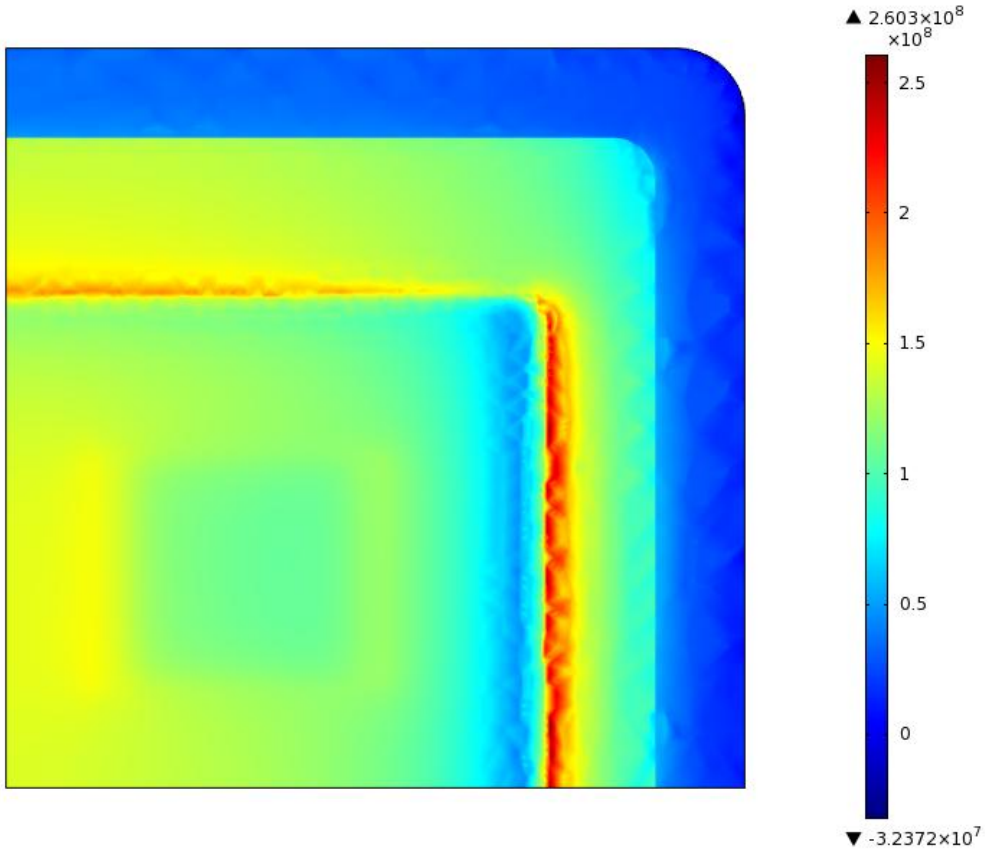

Figure 5.8 Cross-Section X-Tensor Stress Distribution Through AlN at -65°C

Compression is observed only in the free edges of the semiconductors and the aluminum layer, as well as in the top of the protruding wall of the baseplate. The magnitudes of these compressive stresses increase with lower temperatures with the greatest compression of about 70 MPa seen in the aluminum at -65°C. At this temperature, both the MOSFETs and the baseplate experience compressive stresses of approximately 10 MPa. The compressive behavior of these layers at -65°C is not of concern for the observed stresses are well below their respective material limits, but unfortunately compression is not the dominant behavior in the module under these conditions.

As stated before, most of the module experiences tension under these harsh conditions, with the greatest tensile stresses located in the AlN ceramic where it is bonded to the aluminum trace layer. The stresses observed in this layer during high temperature operation were tolerable because they were compressive and ceramics perform exceptionally well under this type of loading, but ceramics do not perform nearly as well under tensile conditions. The maximum tension observed in the ceramic is 404 MPa, which is roughly 50% times greater than its tensile strength of 270 MPa. Note that again the maximum stress seen in the cross-section of this layer provided above is less than that near the surface of the material where it is bonded to the aluminum, which again emphasizes the importance of minimizing CTE mismatch between layers.

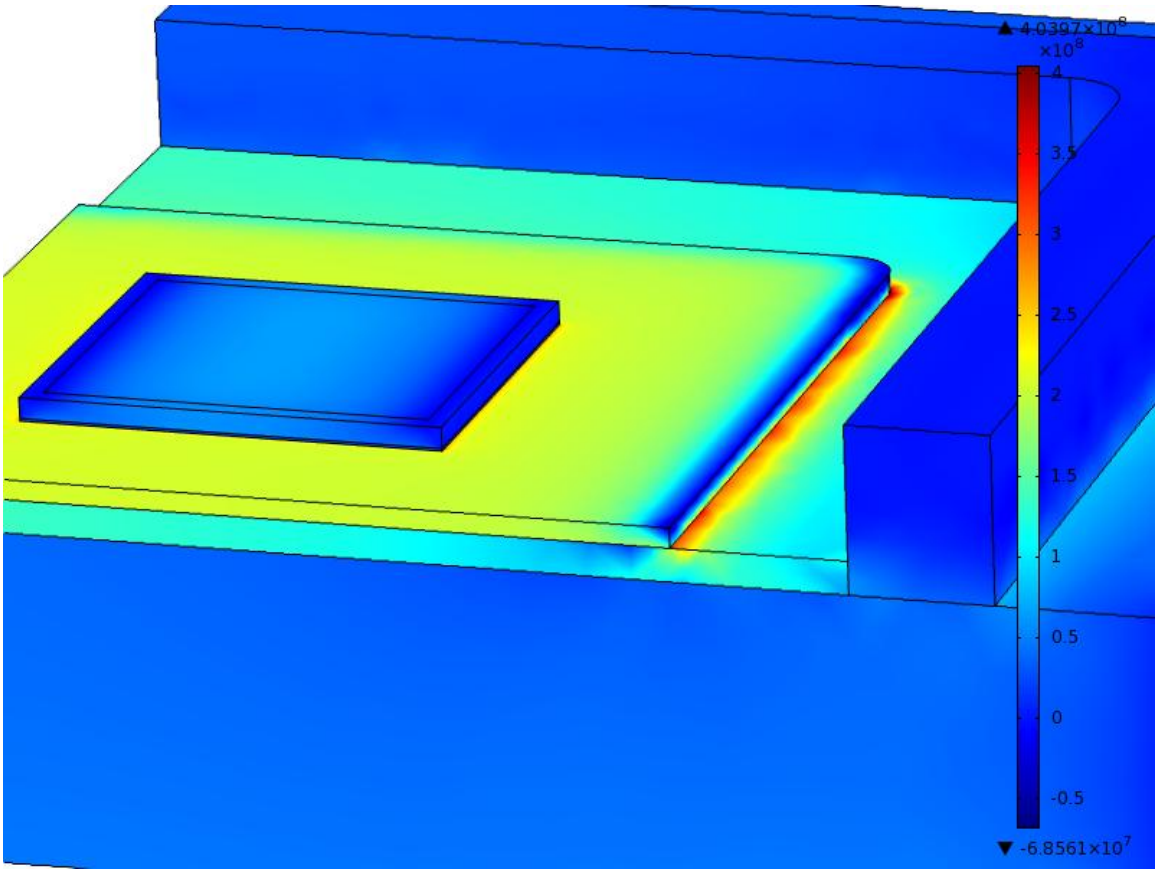

Figure 5.9. X-Tensor Stress Distribution at -65°C

The AlN is not the only layer that exceeds its material's strength, however, as it is observed that the MMC baseplate experiences a tensile stress of about 130 MPa. This is approximately 30% greater than the tensile strength of 103 MPa provided by the manufacturer. The greatest tension in the aluminum layer is observed at the boundary where it is bonded to the ceramic and has a magnitude of about 344 MPa. The aluminum experiences a tensile stress of about 270 MPa at the boundary where the MOSFETs are bonded, which also exceeds its tensile strength.

Although most of the layers in the module experience stresses at -65°C that will cause failure, the SiC MOSFETs and the silver glass are the two layers that do not bring up concern. The tension in the middle of the dies is about 70 MPa, which is about three times lower than the tensile strength of SiC, and although material stress limits for the silver glass are unknown this layer experiences a very uniform tensile stress of about only 20 MPa.

Although the module cannot survive at the lowest target temperature, it was still important to identify the lowest temperature at which the module can safely exist. Simulations were performed where the entire module was subjected to ambient temperatures of 0°C, -20°C, and -40°C. From the results of these simulations it was observed that the module behavior is always identical to that at -65°C, but the stresses – both compressive and tensile – increase as the ambient temperature decreases. Figure 5.10 below demonstrates the trend of stresses in each layer according to the temperature of the module. Note that only the tensile stresses are included in the figure because even the greatest compressive stresses observed at any temperature were well under their material strength and are not a cause of concern. According to the figure, and comparing these values to the strength of each material, it is seen that the module is limited to a temperature of about -38°C, where at this temperature the AlN layer reaches its tensile limit and will experience some form of failure.

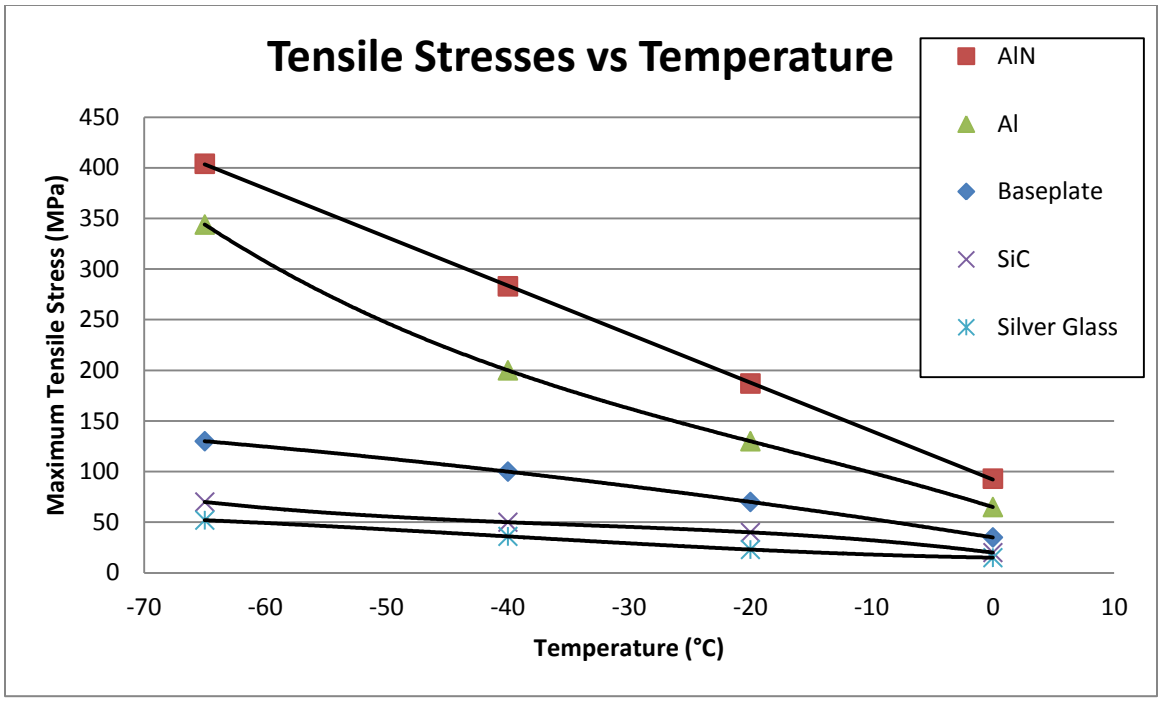

Figure 5.10. Maximum Tensile Stresses in Each Layer vs Temperature

Note that the goal of this work is not to provide usage guidelines for this module, and no recommendations for what can be considered a safe ambient temperature will be provided. With no previous studies performed on the mechanical response of the module, the goal of this research is to instead provide a first account of the expected module behavior under these very low temperatures. Also note that these simulations represent a non-operational state. When operating even at the nominal current the semiconductors will produce heat that will spread throughout the module and – based on previous observations – will most likely alleviate the tensile stresses that are the cause of failure in the module under these low-temperature conditions. This work does not include these considerations and only presents the stress state of the module when in storage or in a non-operational state.

6. Conclusion

6.1 Conclusion

As the aviation and aerospace industries move towards more electric aircraft, the demands of the on-board power distribution systems are consistently growing. In order to meet these demands, the development of reliable, fast-interrupting circuit breakers is essential to continue protecting the wires and components of these electrical systems. Because conventional electro-mechanical circuit breakers cannot meet these requirements, the solid-state power controller has been developed for fault current protection of these systems. These devices are able to detect and interrupt a fault current in nanoseconds, preventing this current from surging through the rest of the PDS and damaging the components of the system.

This research presented a SSPC of the highest power density currently in development, designed to operate at a nominal current rating of $96A_{DC}$ and be able to reliably protect against a maximum fault current rating of $960A_{DC}$. This module has been developed in conjunction with DensePower, LLC, and is able to operate at such high power densities by being able to operate up to a junction temperature of 350°C from 105°C. Operation up until this temperature is achieved through the use of a silicon

carbide-based MOSFET and a heavily aluminum-based packaging that promotes steady and efficient heat flow away from the switching device where it is generated.

Through simulation work using COMSOL Multiphysics, the transient thermal and mechanical behavior of the module was studied, with emphasis on determining the sustaining time of the MOSFETs during a fault current and the stresses in the module due to the expansion of the layers as a result of heating.

From the results of the transient thermal simulations, it was determined that the module (more specifically the MOSFETs) can operate for a sustaining time of 3 milliseconds when subjected to the maximum rated fault current of $960A_{DC}$. Cross-sectional diagrams of the temperature distribution at 3ms were used to demonstrate the efficient spread of heat through the module layers and calculations were performed to quantify the ability of the module to provide efficient thermal management. Through these calculations it was found that approximately 80% of the energy produced within the active volume of each MOSFET is dispersed through the module, and this efficient thermal management is directly responsible for the sustaining time of the power switch devices. These results demonstrate the effectiveness of the Al-based packaging and justify the decision to go with a mono-material approach to the packaging.

Simulations were also performed to study the thermo-mechanical behavior of the module under the same conditions. As the module heats up due to resistive losses, stresses are produced due to the mismatch of thermal expansion coefficients between the layers. All of the stresses observed in the module layers were under the

compressive or tensile limits of their respective material, with the aluminum layer causing the greatest concern as it exhibited a factor of safety of roughly 1.5.

In order to fully understand the behavior of the module, simulations were performed to study the mechanical response of the module due to the fabrication process, where the first three layers are fired together at approximately 700°C and allowed to cool down to room temperature. It was determined that the pre-stresses in the module layers are not very sensitive to the cooling rate, and were found to be well under the limits of their respective materials. These stresses are low enough to be admissible and the results from the transient simulations can be considered accurate and credible.

Lastly, the entire module was cooled down to temperatures as low as -65°C so that the behavior of the layers could be studied at this military application range. Under these conditions of very low ambient temperatures tension dominated the module and limited its usage to a temperature of about -38°C. Tensile stress versus temperature data was provided for each layer in a graph so that the behavior of the module in response to low temperatures could be easily understood. It was observed that the AlN ceramic experienced the greatest stresses and would be the first to failure as the ambient temperature decreased.

This research was a necessary step in the development of a solid-state power controller. No previous work has investigated the behavior of a complete SSPC module, especially in response to its true operating conditions, namely the resistive losses

resulting from a very high fault current. While much more work can be performed on this particular module, this research was important in that it established a precedent for a solid-state power controller that can operate to a very high junction temperature at an extremely high power density. This work provided some of the very first characterization of a full SSPC module by documenting its thermal management capabilities and the resultant sustaining time of its power switching semiconductors. This work also characterized the mechanical behavior of the module by documenting the stresses generated in the module under various conditions. This allowed for identification of areas in the module that are most susceptible to failure and for determination of the lowest temperatures that this module may be subjected.

6.2 Future Work

Although this research provides an excellent characterization of the proposed module, it should only be used as a foundation for the development of this module for there is much more work that can be performed.

Remember that the relation between temperature and the on-state resistance of the semiconductors was created by extrapolating the manufacturer data out to the desired temperature range. Because the thermal portrayal of the module is so heavily dependent upon this relation, experiments should be performed to provide an accurate account of the on-state resistance behavior at higher temperatures. This would allow for an even more accurate representation of the heating effect in the MOSFETs.

Although most of the layers in the module are completely set, DensePower has expressed interest in using a baseplate with a slightly different composition. The manufacturer has a several different MMCs that can be easily substituted into the module. These materials have not been looked into, but it is the hope that one may exhibit a CTE that better matches the AlN layer and therefore may help mitigate the stresses that build up in the ceramic. Performing the simulations again with different material properties for the baseplate would be an easy next step that has the possibility of improving the mechanical response of the module.

Although some of the parameters of the module can be changed and the simulations performed again, an important next step would be to build a physical prototype of the SSPC module and perform experimental tests. Initially these tests could be used to verify the sustaining time of the MOSFETs and the thermal management capabilities of the modules shown by the simulations. These tests could also be used to verify the mechanical results presented in this research. For example, a strain gauge could be placed on the top surface of the AlN ceramic right near the boundary where the aluminum trace layer is bonded. This would allow for a quick and easy comparison of some of the most crucial stresses observed by the simulations.

Experimental testing would also be useful in determining not only the mode of failure in the module layers themselves, but also in studying the behavior of the bonds between layers. The simulation work assumes that the layers are perfectly bonded together with no voids or imperfections which may be present in the actual module.

The simulations also only show the stresses in the layers themselves and cannot give a representation of the forces acting on the bonding between layers as they expand/contract and pull on one another. Experimental testing would be essential to studying these effects.

One last major study that can be done is to investigate the effects of thermal cycling on the module. This research demonstrates the response of the module to only one fault current load, and it is understood that the behavior of the module may drastically change with successive loads. The results of thermal cycling tests and/or simulations would be crucial to defining the overall reliability of the module.

Reference

[1] J. S. Cloyd, “Status of United States Air Force's More Electric Aircraft Initiative”, IEEE Aerospace and Electronic Systems Magazine, Vol. 13, No. 4, pp. 17-22, 1998.

[2] A. Barrado, D. Izquierdo, M. Sanz, C. Raga, A. Lazaro, “Behavioural Modeling of Solid State Power Controllers (SSPC) for Distributed Power Systems”, Proceedings of the 2009 IEEE Applied Power Electronics Conference (APEC), Washington, DC, February 15-19, 2009.

[3] K. Emadi, M. Ehsani, “Aircraft Power Systems: Technology, State of the Art, and Future Trends”, IEEE Aerospace and Electronic Systems Magazine, Vol. 15, No. 1, pp. 28-32, 2000.

[4] J.A. Rosero, J.A. Ortega, E. Aldabas, L. Romeral, “Moving Towards a More Electric Aircraft”, IEEE Aerospace and Electronic Systems Magazine, Vol. 22, No. 3, pp. 3-9, 2007.

[5] R. Jayabalan, B. Fahimi, A. Koenig, S. Pekarek, “Applications of Power Electronics-Based Systems in Vehicular Technology: State-of-the-Art and Future Trends”, Proceedings of the 2004 IEEE Power Electronics Specialists Conference, Aachen, Germany, pp. 1887-1894, 2004.

[6] M.A. Maldonado, N.M. Shah, K.J. Cleek, G.J. Korba, “Power Management and Distribution System for a More-Electric Aircraft (MADMEL) – Program Status”, IEEE Aerospace and Electronics Systems Magazine, Vol. 14, No. 12, pp. 3-8, December, 1999.

[7] M. Howse, “All Electric Aircraft”, Power Engineering, Vol. 17, No. 4, pp. 35-37, August 2003.

[8] D. Izquierdo, A. Barrado, M. Sanz, C. Fernandez, P. Zumel, “Modeling Methods for Solid State Power Controllers”, Proceedings of the 2009 International Compatibility and Power Electronics Conference (CPE), Badajoz, Spain, May 20-22, pp. 265-270, 2009.

[9] X. Feng, “SiC Based Solid State Power Controller”, Dissertation, University of Kentucky, August 24, 2007.

[10] Y.V. Panov, F.C. Lee, “Modeling and Stability Analysis of a DC Power System with Solid State Power Controllers”, Proceedings of the 1996 Applied Power Electronics Conference and Exposition (APEC), Eleventh Annual, Vol. 2 , pp. 685-691, 1996.

[11] S.N. Friedman, " Robust/Low Cost Solid-State Remote Power Controller (RPC) Technology is Here", Proceedings of the 1999 Digital Avionics Systems Conference (DASC), St. Louis, Missouri, October 24-29, Vol. 1, pp. 3.B.4.1-3.B.4.7, 1999.

[12] T.R. Boldt, G.L. Dunn, D.E. Hankins, P.J. Leong, I.S. Mehdi, "Advanced Aircraft Electrical System Control Technology Demonstrator, Phase I: Requirements Analysis and Preliminary Design, Phase II: Detailed Design", Boeing Military Airplane Company, Seattle, Washington, May 1983.

[13] D. Nemir, A. Martinez, "Arc Fault Management Using Solid State Switching", Proceedings of the 2004 Power Systems Conference, Reno, Nevada, November 2004.

[14] D. Izquierdo, A. Barrado, C. Raga, M. Sanz, P. Zumel, A. Lazaro, "Protection Devices for Aircraft Electrical Power Distribution Systems: A Survey", Proceedings of 2008 Annual Conference of the IEEE Industrial Electronics Society (IECON), November, pp. 903-908, 2008.

[15] I. Khan, M. Critchley, "Arc Fault Detector", Leach International, 2002.

[16] W. Liu, A.Q. Huang, "A Novel High Current Solid State Power Controller", Proceedings of 1993 Annual Conference of the IEEE Industrial Electronics Society (IECON), November, pp. 1306-1310, 2005.

[17] T. Kulworawanichpong, "Modeling of Solid-state Circuit Breakers using MATLAB's Power System Blockset", International Journal of Mathematics and Computers in Simulation, Vol. 2, No. 3, pp. 236-245, 2008.

[18] W. Pusorn, W. Srisongkram, W. Subsingha, S. Deng-em, P.N. Boonchiam, "Low Cost AC Solid State Circuit Breaker", Proceedings of the 2007 International Conference on Power Electronics and Drive Systems (PEDS), Bangkok, Thailand, November 27-30, pp. 1851-1856, 2007.

[19] R. Spyker, D.L. Schweickart, J.C. Horwath, L.C. Walko, D. Grosjean, "An Evaluation of Diagnostic Techniques Relevant to Arcing Fault Current Interrupters for Direct Current Power Systems in Future Aircraft", Proceedings of the 2005 Electrical Insulation Conference and Electrical Manufacturing Expo, October, pp. 146-150, 2005.

[20] SAE Standard AS5692, "Arc Fault Circuit Breaker (AFCB), Aircraft, Trip Free Single Phase 115 VAC, 400Hz – Constant Frequency", Issued October 14, 2004.

[21] E.L. Wellner, “Circuit Breaker Including an Arc Fault Trip Actuator Having an Indicator Latch and a Trip Latch”, United States Patent 6522228, February 18, 2003.

[22] T.R. Maher, “Solid State Power Controller”, United States Patent 5723915, March 3, 1998.

[23] R.Y. Kinoshita, “Solid State DC Power Switch”, United States Patent 4709160, August 25, 1986.

[24] Y.B. Guo, D.P. Bhat, A. Aravamudhan, D.C. Hopkins, D.R. Hazelmyer, “High Current and Thermal Transient Design of a SiC SSPC for Aircraft Application”, Proceedings of the 2011 Applied Power Electronics Conference (APEC), Ft. Worth, Texas, March 6-11, 2011.

[25] C.H. Flurscheim, “Power Circuit Breaker Theory and Design”, London, U.K.: Peter Peregrinus, 1975.

[26] T.E. Browne, “Circuit Interruption: Theory and Techniques”, New York: Marcel Dekker, 1984.

[27] D. Planson, D. Tournier, P. Bevilacqua, N. Dheilly, H. Morel, C. Raynaud, M. Lazar, D. Bergogne, B. Allard, J. P. Chante, “SiC Power Semiconductor Devices for New Applications in Power Electronics”, Proceedings of the 2008 International Power Electronics and Motion Control Conference (EPE-PEMC), pp. 2457-2463, 2008.

[28] A. Barrado, D. Izquierdo, C. Raga, A. Lazaro, M. Sanz, “SSPC Model with Variable Reset Time, Environmental Temperature Compensation and Thermal Memory Effect”, Proceedings of the 2008 IEEE Applied Power Electronics Conference (APEC), pp. 1716-1721, 2008.

[29] J.C. Zolper, “Emerging Silicon Carbide Power Electronics Components”, Proceedings of the 2005 Applied Power Electronics Conference (APEC), Austin, Texas, March 6-10, pp. 11-17, 2005.

[30] K.A. LaBel, R.K. Barry, K. Castell, H.S. Kim, C.M. Seidleck, “Implications of Single Event Effect Characterization of Hybrid DC-DC Converters and a Solid State Power Controller”, IEEE Transactions on Nuclear Science, Vol. 42, pp. 1957-1963, December 1995.

[31] J.B. Casady, R.W. Johnson, “Status of Silicon Carbide (SiC) as a Wide-Bandgap Semiconductor for High-Temperature Applications: A Review”, Solid-State Electronics, Vol. 39, No. 10, pp. 1409-1422, 1996.

[32] D.S. Hart, G.B. Prickett, C.R. Schwarz, M. Mohadjer, “A Solid State Power Controller Module for the International Space Station Express Rack”, Proceedings of the 1997 Energy Conversion Engineering Conference (IECEC), Honolulu, HI, pp. 280-285, 1997.

[33] X. Xia, “Dynamic Power Distribution Management for All Electric Aircraft”, Thesis, Cranfield University, January, 2011.

[34] W. Wondrak, R. Held, E. Niemann, U. Schmid, “SiC Devices for Advanced Power and High-Temperature Applications”, IEEE Transactions on Industrial Electronics, Vol. 48, No. 2, pp. 307-308, 2001.

[35] B. Dobrucky, P. Spanik, R. Sul, “Improvement of Power Electronic Structure Characteristics Using SiC Technology Overview”, Komunikacie Communications, pp. 34-38, 2006.

[36] L.M. Tolbert, B. Ozpineci, S.K. Islam, F.Z. Peng, “Impact of SiC Power Electronic Devices for Hybrid Electric Vehicles”, Proceedings of the 2002 Future Car Congress, Arlington, Virginia, June 3-5, SAE Paper Number 2002-01-1904, 2002.

[37] C.E. Weitzel, J.W. Palmour, C.H. Carter, Jr., K. Moore, K.J. Nordquist, S. Allen, C. Thero, M. Bhatnagar, “Silicon Carbide High-Power Devices”, IEEE Transactions on Electron Devices, Vol. 43, No. 10, pp. 1732-1741, October 1996.

[38] F.P. McCluskey, R. Grzybowski, T. Podlesak, “High Temperature Electronics”, CRC Press, 1997.

[39] L.D. Stevanovic, D.S. Matocha, P.A. Losee, J.S. Glaser, J.J. Nasadoski, S.D. Arthur, “Recent Advances in Silicon Carbide MOSFET Power Devices”, Proceedings of IEEE Applied Power Electronics Conference (APEC), pp. 401-407, 2010.

[40] S. Bontemps, A. Calmels S.D. Round, J.W. Kolar, “Low Profile Power Module Combined with State of the Art MOSFET Switches and SiC Diodes Allows High Frequency and Very Compact Three-Phase Sinusoidal Input Rectifiers”, Proceedings of the 2007 Conference for Power Electronics, Intelligent Motion, and Power Quality (PCIM), Nuremberg, Germany, 2007.

[41] A.B. Lostetter, F. Barlow, A. Elshabini, “An Overview to Integrated Power Module Design for High Power Electronics Packaging”, Microelectronics Reliability, Vol. 40, pp. 365-379, 2000.

[42] T.R. Sahroni, S. Sulaiman, I. Romli, M.R. Salleh, H.A. Ariff, “Nonlinear Thermal Expansion Model for SiC/Al”, World Academy of Science, Engineering, and Technology (WASET), Vol. 78, 2011.

[43] S. Azzopardi, J.M. Thebaud, E. Woirgard, C. Zardini, P. Sable, "Al/SiC Baseplate Hybrid Power Modules: Evaluation of the Thermomechanical Performances", Proceedings of the 1998 IEEE International Workshop on Integrated Power Packaging (IWIPP), Chicago, Illinois, September 17-19, pp. 74-78, 1998.

[44] J.M. Fusaro, G.L. Romero, P. Rodriguez, J.L. Martinez, Jr., "Thermal Characterization of DBC and MMC Stacks for Power Modules", Proceedings of the 1996 Industry Applications Conference, October 6-10, San Diego, California, pp. 1411-1417, 1996.

[45] L. Dupont, Z. Khatir, S. Lefebvre, S. Bontemps, "Effects of Metallization Thickness of Ceramic Substrates on the Reliability of Power Assemblies Under High Temperature Cycling", Microelectronics Reliability, Vol. 46, pp. 1766-1771, 2006.

[46] L.Dupont, Z. Khatir, S. Lefebvre, R. Meuret, B. Parmentier, S. Bontemps, "Electrical Characterizations and Evaluation of Thermo-Mechanical Stresses of a Power Module Dedicated to High Temperature Applications", European Conference on Power Electronics and Applications, Dresden, 2005.

[47] Y.B. Guo, "Development of a High Current High Temperature SiC MOSFET Based Solid-State Power Controller", Thesis, Buffalo University, Defended December 13, 2010.

[48] D. C. Hopkins, Y. B. Guo, H. E. Dwyer, J. D. Scofield, "Development of a SiC SSPC Module with Advanced High Temperature Packaging," Proceedings of the 2010 High Temperature Electronics Conference (HiTEC), Albuquerque, New Mexico, May 11-13, 2010.

[49] Y.B. Guo, D.P. Bhat, A. Aravamudhan, D.C. Hopkins, D.R. Hazelmyer, "Results for an Al/AlN Composite 350°C SiC Solid-State Circuit Breaker Module", Proceedings of the 2012 Applied Power Electronics Conference (APEC), Orlando, Florida, February 5-9, 2012.

[50] D.C. Hopkins, D.W. Kellerman, R.A. Wunderlich, C. Basaran, J. Gomez, "High-Temperature, High-Density Packaging of a 60kW Converter for >200°C Embedded Operation", Proceedings of the 2006 IEEE Applied Power Electronics Conference (APEC), Dallas, Texas, March 19-23, pp. 7, 2006.

[51] D.C Hopkins, D.W. Kellerman, C. Basaran, J. Gomez, "Aluminum-Based High-Temperature (>200°C) Packaging for SiC Power Converters", Proceedings of the 2006 International Symposium on Microelectronics (IMAPS), San Diego, California, October 8-12, pp. 734-741, 2006.

[52] B. Ozpineci, L.M. Tolbert, “Comparison of Wide-Bandgap Semiconductors for Power Electronics Applications”, Oak Ridge National Laboratory, Oak Ridge, Tennessee, December 12, 2003.

[53] T.P. Chow, V. Khemka, J. Fedison, N. Ramungul, K. Matocha, Y. Tang, R.J. Gutmann, “SiC and GaN Bipolar Power Devices”, Solid-State Electronics, Vol. 44, pp. 277-301, 2000.

[54] S. Dimitrijev, P. Jamet, “Advances in SiC MOSFET Technology”, Microelectronics Reliability, Vol. 43, pp. 225-233, 2003.

[55] J.C. Zolper, “A Review of Junction Field Effect Transistors for High-Temperature and High-Power Electronics”, Solid-State Electronics, Vol. 42, No. 12, pp. 2153-2156, 1998.

[56] W. Wondrak, “Physical Limits and Lifetime Limitations of Semiconductor Devices at High Temperatures”, Microelectronics Reliability, Vol. 39, pp. 1113-1120, 1999.

[57] J.L. Hudgins, G.S. Simins, E.S. Santi, M.A. Khan, “An Assessment of Wide Bandgap Semiconductors for Power Devices”, IEEE Transactions on Power Electronics, Vol. 18, pp. 907-914, May 2003.

[58] T. Munson, “Mesh Shape-Quality Optimization Using the Inverse Mean-Ratio Metric”, Argonne National Laboratory, Argonne, Illinois, June 2005.

[59] R. Li, “On Multi-Mesh *H*-Adaptive Methods”, Journal of Scientific Computing, Vol. 24, No. 3, pp. 321-341, September 2005.